PHYSICAL REVIEW D **90,** 074018 (2014)

Glauber gluons in spectator amplitudes for $B \to \pi M$ decays

Hsiang-nan Li[1,*] and Satoshi Mishima[2,†]

[1]*Institute of Physics, Academia Sinica, Taipei, Taiwan 115, Republic of China; Department of Physics, Tsing-Hua University, Hsinchu, Taiwan 300, Republic of China; and Department of Physics, National Cheng-Kung University, Tainan, Taiwan 701, Republic of China*

[2]*Dipartimento di Fisica, Università di Roma "La Sapienza", I-00185 Roma, Italy and SISSA, Via Bonomea 265, I-34136 Trieste, Italy*

(Received 8 August 2014; published 15 October 2014)

We extract the Glauber divergences from the spectator amplitudes for two-body hadronic decays $B \to M_1 M_2$ in the k_T factorization theorem, where M_2 denotes the meson emitted at the weak vertex. Employing the eikonal approximation, the divergences are factorized into the corresponding Glauber phase factors associated with the M_1 and M_2 mesons. It is observed that the latter factor enhances the spectator contribution to the color-suppressed tree amplitude by modifying the interference pattern between the two involved leading-order diagrams. The first factor rotates the enhanced spectator contribution by a phase, and changes its interference with other tree diagrams. The above Glauber effects are compared with the mechanism in elastic rescattering among various $M_1 M_2$ final states, which has been widely investigated in the literature. We postulate that only the Glauber effect associated with a pion is significant, due to its simultaneous roles as both a $q\bar{q}$ bound state and a pseudo-Nambu-Goldstone boson. Treating the Glauber phases as additional inputs in the perturbative QCD (pQCD) approach, we find a good fit to all the $B \to \pi\pi$, $\pi\rho$, $\pi\omega$, and πK data, and resolve the long-standing $\pi\pi$ and πK puzzles. The nontrivial success of this modified pQCD formalism is elaborated.

DOI: 10.1103/PhysRevD.90.074018 PACS numbers: 13.25.Hw, 12.38.Bx, 12.39.St

I. INTRODUCTION

The known $B \to \pi\pi$ and $B \to \pi K$ puzzles have stimulated a lot of discussions in the literature: the measured $B^0 \to \pi^0\pi^0$ branching ratio [1] is several times larger than the naive expectation, and the measured direct CP asymmetry in the $B^\pm \to \pi^0 K^\pm$ decays dramatically differs from the $B^0 \to \pi^\mp K^\pm$ one. It has been pointed out that these puzzles are sensitive to the least-understood color-suppressed tree amplitudes C [2–4]. Other similar discrepancies were also observed: the $B^0 \to \pi^0\rho^0$ branching ratios from the perturbative QCD (pQCD) and QCD factorization (QCDF) approaches, being sensitive to C, are lower than the data [5–7]. However, the estimate of C from pQCD is well consistent with the measured $B^0 \to \rho^0\rho^0$ branching ratio [8]. Proposals resorting to new physics [9–21] mainly resolved the πK puzzle without addressing the peculiar feature of C in the $\pi^0\pi^0$, $\pi^0\rho^0$, and $\rho^0\rho^0$ modes, while those resorting to QCD effects are usually strongly constrained by the $\rho\rho$ data [22]. The recent resolution of the $B \to \pi K$ puzzle by means of the so-called Pauli blocking mechanism seems to lack solid theoretical support [23]. This exemplifies the difficulty of this subject.

Motivated by the above puzzles, we have carefully investigated the subleading contributions to the amplitudes C and their impact on the $B \to \pi\pi$, πK decays in the pQCD approach based on the k_T factorization theorem [24,25]. For example, the next-to-leading-order (NLO) contributions from the vertex corrections, the quark loops, and the magnetic penguin have been calculated [26,27]. Nevertheless, once a mechanism identified for C respects the conventional factorization theorem, it is unlikely to be a resolution due to the $B \to \rho\rho$ constraint mentioned above [8]. This is the reason why the above NLO corrections could not resolve the puzzles completely, though the consistency between the pQCD predictions and the data was improved. For a similar reason, higher-order corrections evaluated in QCDF [28]—which obey the collinear factorization—cannot resolve the $B \to \pi\pi$ puzzle either. In a recent work [29] we have analyzed high-order corrections to the spectator diagrams in the k_T factorization theorem, and found a new type of infrared divergence, which are called Glauber gluons [30]. The all-order summation of the Glauber gluons leads to a phase factor, which modifies the interference between the spectator diagrams for C. We postulated that only the Glauber factors associated with a pion give significant effects, due to its simultaneous roles as both a $q\bar{q}$ bound state and a pseudo-Nambu-Goldstone (NG) boson [31]. It was then demonstrated that the Glauber effect, enhancing the magnitude of C, partially resolved the $B \to \pi\pi$ and $B \to \pi K$ puzzles. Our prediction for the $B^0 \to \pi^0\pi^0$ branching ratio around 1.0×10^{-6} [29] turns out to be consistent with the recent Belle data $(0.90 \pm 0.12 \pm 0.10) \times 10^{-6}$ [32].

*hnli@phys.sinica.edu.tw
†Satoshi.Mishima@roma1.infn.it

The above progress implies that the Glauber gluons in the k_T factorization theorem deserve a thorough study. In this paper we shall examine whether the Glauber divergences in the spectator diagrams for the $B \to M_1 M_2$ decay, where M_2 denotes the meson emitted at the weak vertex, have been extracted completely, and whether the same Glauber effect improves the consistency of the pQCD predictions with other data involving the pion, such as the $B \to \pi\rho, \pi\omega$ data. It will be shown that there exist Glauber divergences associated with the M_1 meson, in addition to those associated with the M_2 meson [29]. The all-order organization of the Glauber divergences follows the standard procedures, relying on the eikonal approximation for soft gluons. The resultant Glauber factor $\exp(-iS_{e1})$ from M_1 is the same for the two leading-order (LO) spectator diagrams. The Glauber factor from M_2 carries opposite phases, namely, $\exp(iS_{e2})$ for one diagram, and $\exp(-iS_{e2})$ for another. Therefore, they have different impacts on the amplitude C: the latter enhances the spectator contribution to C by modifying the interference pattern between the two LO diagrams (as mentioned before), whereas the former rotates the enhanced spectator contribution by a phase, and changes its interference with other tree diagrams. The correspondence between the Glauber factors and the mechanism in elastic rescattering among various $M_1 M_2$ final states will be made explicit, including the singlet exchange and the charge exchange, which have been widely explored in the literature [33,34].

The Glauber factors $\exp(-iS_{e1})$ (as $M_1 = \pi$), and $\exp(\pm iS_{e2})$ (as $M_2 = \pi$) are introduced into the pQCD factorization formulas for the spectator diagrams in the $B \to \pi\pi$, $\pi\rho$, $\pi\omega$, and πK modes (a total of 13 modes), and the phases S_{e1} and S_{e2} are treated as additional inputs. It turns out that the equal value $S_{e1} = S_{e2} \approx -\pi/2$ leads to a good fit to all the $B \to \pi M$ data. It will be observed that the Glauber effects give NLO pQCD predictions for the $B^0 \to \pi^+\pi^-$, $B^+ \to \pi^+\pi^0$, and $B^0 \to \pi^0\pi^0$ branching ratios that agree well with the data. In particular, the rotation of the spectator amplitude by $\exp(-iS_{e1})$ is crucial for enhancing the ratio of the $B^+ \to \pi^+\pi^0$ branching ratio over the $B^0 \to \pi^+\pi^-$ one; this ratio depends on both the color-allowed tree amplitude T and the color-suppressed tree amplitude C, so the relative phase between them matters. It is a nontrivial success that all the $B \to \pi\pi$, $\pi\rho$, and πK puzzles mentioned before are resolved at the same time by introducing two Glauber phases.

In Sec. II we construct the standard meson wave functions for the $B \to M_1 M_2$ decays in the k_T factorization theorem, and analyze the residual infrared divergences caused by the Glauber gluons in the NLO spectator diagrams. The Glauber gluons associated with the M_1 and M_2 mesons are then factorized into the Glauber factors $\exp(-iS_{e1})$ and $\exp(\pm iS_{e2})$, respectively. In Sec. III we investigate the numerical impacts of the Glauber factors on the $B \to \pi\pi$, $\pi\rho$, $\pi\omega$, and πK decays by presenting NLO pQCD predictions as contour plots in the S_{e1}-S_{e2} plane. The agreement between the predictions and the data for the branching ratios and direct CP asymmetries as $S_{e1} = S_{e2} \approx -\pi/2$ is highlighted. Section IV contains the conclusion. The existence of the Glauber divergences is illustrated in the Appendix by means of the Feynman parametrization of loop integrands.

II. FACTORIZATION OF GLAUBER GLUONS

It was pointed out in Ref. [30] that the k_T factorization theorem holds for simple processes like deeply inelastic scattering, but residual infrared divergences from the Glauber region may appear in complicated QCD processes like high-p_T hadron hadroproduction. To factorize the collinear gluons associated with, say, one of the initial-state hadrons, one eikonalizes the particle lines to which the collinear gluons attach. The eikonal lines from other hadrons should cancel in order to maintain the universality of the parton distribution function under consideration. However, the required cancellation is not exact in the k_T factorization, leading to imaginary infrared logarithms, though it is in the collinear factorization. It has been demonstrated that the residual divergences can be factorized into a Glauber factor for low-p_T hadron hadroproduction: the contour of a collinear gluon momentum can be deformed away from the Glauber region at low p_T, such that the usual eikonalization still holds [35]. The above investigation was then extended to two-body hadronic B-meson decays $B \to M_1 M_2$, and the residual infrared divergences in a spectator amplitude associated with the M_2 meson were found and factorized into the same Glauber factor [29]. Note that the k_T factorization for a factorizable emission amplitude, i.e., a B-meson transition form factor, was proven in Ref. [36].

In this section we shall perform a thorough study of the infrared divergences in the spectator diagrams at the one-loop level of the k_T factorization, following reasoning different from that in Ref. [29]. Both the infrared divergences—which are absorbed into the standard meson wave functions—and the residual infrared divergences from the Glauber gluons associated with the mesons M_1 and M_2 will be extracted. Since we have postulated that only the Glauber effect from the pion is significant, it is not necessary to discuss the Glauber divergences associated with the B meson. In principle, the Glauber gluons also exist in spectator penguin diagrams and in nonfactorizable annihilation diagrams, in which the hard gluon is emitted by the b quark or by the spectator quark in the B meson. As explained in Ref. [29], these diagrams are larger at LO, so they are more stable against subleading corrections. The Glauber effect is expected to be more significant in the spectator tree amplitudes, because of their tininess at LO.

Consider the $B(P_B) \to M_1(P_1) M_2(P_2)$ decay, where P_B, P_1, and P_2 represent the momenta of the B, M_1, and M_2 mesons, respectively. For convenience, we choose

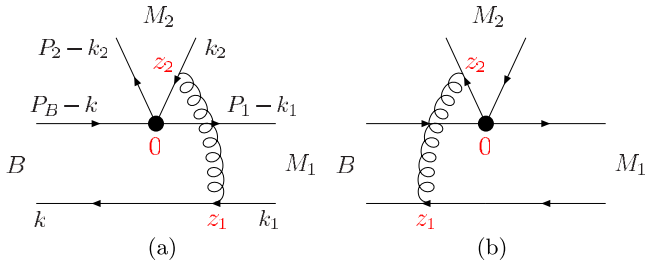

FIG. 1 (color online). LO diagrams for a spectator amplitude.

$P_B = (P_B^+, P_B^-, \mathbf{0}_T)$ with $P_B^+ = P_B^- = m_B/\sqrt{2}$, with m_B being the B-meson mass, and P_1 (P_2) is in the plus (minus) direction. The parton four-momenta k, k_1, and k_2 are labeled in Fig. 1(a). After performing loop integrations, we keep $k^- = xP_B^-$, $k_1^+ = x_1 P_1^+$, $k_2^- = x_2 P_2^-$, and the transverse components k_T that appear in the hard kernel for the b-quark decay. The order of magnitude $x_2 \sim 0.5$, $x_1 \sim 0.3$, $x \sim 0.1$, $m_B \sim 5$ GeV, and $k_T \lesssim 1$ GeV implies the hierarchy among the scales involved in exclusive B-meson decays in the small-x region [37],

$$m_B^2, x_2 m_B^2 \gg x_1 m_B^2 \gg x m_B^2 \gg x x_1 m_B^2, k_T^2, \tag{1}$$

which will serve as a basis for higher-order analysis below.

We first identify the Glauber gluons associated with the LO spectator tree diagram in Fig. 1(a), originating from the operator O_2 [38]. We start with the set of NLO diagrams with a radiative gluon of momentum l being emitted by the valence quark of M_2, as displayed in Fig. 2. Due to the soft cancellation between the gluons radiated by the valence quark and by the valence antiquark of M_2 [39], only the collinear region where l is collimated to P_2 is relevant here, and the k_T dependence of parton propagators in the B and M_1 mesons is negligible. The propagators of these partons attached to the collinear gluons can then be approximated by the eikonal propagators $1/(l^- \pm i\epsilon)$. For a loop diagram to generate an imaginary Glauber logarithm, a necessary (but not sufficient) condition is that the interval of l^- covers the origin $l^- = 0$. The corresponding integral then contains an imaginary piece,

$$\mathrm{Im}\int_{-a}^{b} dl^- \frac{1}{l^- + i\epsilon} = -\pi \int_{-a}^{b} dl^- \delta(l^-) = -\pi, \tag{2}$$

under the principal-value prescription.

It has been shown that Figs. 2(a)–2(c) do not contain Glauber divergences, and they contribute to the M_2 meson wave function [29]. We take the vertex correction in Fig. 2(a) as an example. The integrand is proportional to

$$\frac{1}{2(P_2^- - k_2^- + l^-)l^+ - |\mathbf{k}_{2T} - \mathbf{l}_T|^2 + i\epsilon} \frac{1}{2l^- l^+ - l_T^2 + i\epsilon} \times \frac{1}{2(P_B^- - k^-)l^+ + 2(P_B^+ - k^+ + l^+)l^- + i\epsilon}, \tag{3}$$

where l denotes the loop momentum, and the transverse-momentum-dependent terms of the virtual b-quark propagator have been neglected in the heavy-quark limit. The contour integration over l^+ indicates that the loop integral does not vanish only for $l^- < 0$: in this range there are poles located in the different half complex planes of l^+. Picking up the pole $l^+ \approx 0 - i\epsilon$ [see the power counting in Eq. (1)] associated with the valence-quark propagator in M_2, namely, the first factor of Eq. (3), the b-quark propagator reduces to the eikonal propagator proportional to $1/(l^- + i\epsilon)$. In the range $l^- < 0$ this propagator does not generate a Glauber divergence according to Eq. (2). Because it is factorized in color flow by itself with the color factor C_F, Fig. 2(a) leads to a Wilson line running from minus infinity to the origin, i.e, the weak vertex, which appears in the definition of the M_2 meson wave function. Similarly, the vertex correction in Fig. 2(b) is free of a Glauber divergence. Figure 2(c), with the collinear

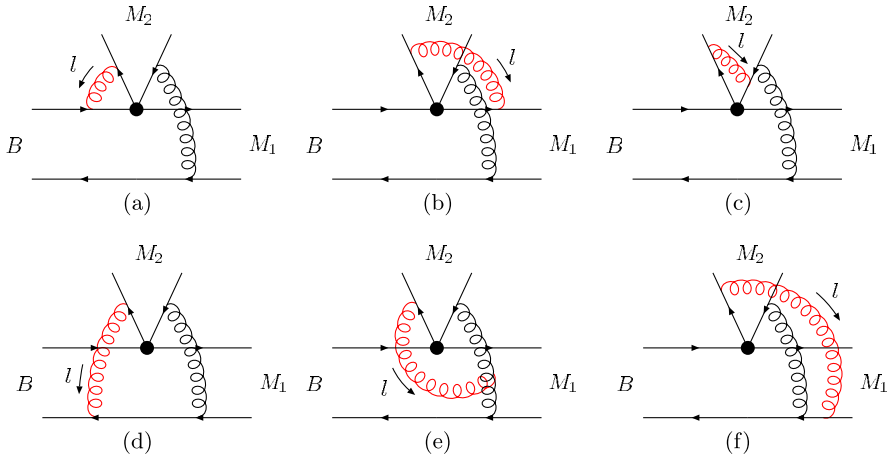

FIG. 2 (color online). NLO diagrams for Fig. 1(a) that are relevant to the factorization of the M_2 meson wave function. Figures 2(d)–2(f) contribute to the Glauber divergences.

gluon attaching to the virtual quark line, does not produce an infrared Glauber divergence: the virtual quark line remains highly off shell by $O(x_1 m_B^2)$ before and after the attachment of the collinear gluon according to Eq. (1), so no Glauber divergence is generated in this diagram.

As was observed in Ref. [29], Figs. 2(d)–2(f) produce residual Glauber divergences under the hierarchical relation in Eq. (1), which demand the introduction of an additional nonperturbative input. The integrand for Fig. 2(d) contains the five denominators

$$[(P_2-k_2+l)^2+i\epsilon][(k+l)^2+i\epsilon][(k-k_1+l)^2+i\epsilon] \times (l^2+i\epsilon)[(k_2-k+k_1-l)^2+i\epsilon]. \tag{4}$$

Nonvanishing contributions come from the ranges $0<l^-<k_2^-$, $-k^-<l^-<0$, and $-(P_2^- - k_2^-)<l^-<-k^-$, where the poles of l^+ are given by

$$l^+ \approx \frac{|\mathbf{l}_T-\mathbf{k}_{2T}|^2}{2(l^- + P_2^- - k_2^-)} - i\epsilon(-i\epsilon,-i\epsilon), \tag{5}$$

$$l^+ = -k^+ + \frac{|\mathbf{l}_T+\mathbf{k}_T|^2}{2(l^- + k^-)} - i\epsilon(-i\epsilon,+i\epsilon), \tag{6}$$

$$l^+ = k_1^+ + \frac{|\mathbf{l}_T-\mathbf{k}_{1T}+\mathbf{k}_T|^2}{2(l^- + k^-)} - i\epsilon(-i\epsilon,+i\epsilon), \tag{7}$$

$$l^+ = \frac{l_T^2}{2l^-} - i\epsilon(+i\epsilon,+i\epsilon), \tag{8}$$

$$l^+ = k_1^+ + \frac{|\mathbf{l}_T-\mathbf{k}_{2T}-\mathbf{k}_{1T}+\mathbf{k}_T|^2}{2(l^- - k_2^-)} + i\epsilon(+i\epsilon,+i\epsilon), \tag{9}$$

respectively. We pick up the first pole $l^+ \sim O(\Lambda_{\rm QCD}^2/m_B) - i\epsilon$, which corresponds to the collinear gluon associated with the valence quark of M_2. It is seen that the allowed range for this pole, $-(P_2^- - k_2^-)<l^-<k_2^-$, covers the origin $l^-=0$, leading to a Glauber divergence from the eikonalized spectator propagator $1/(k+l)^2$ and the on-shell radiative gluon. The other poles, such as those in Eqs. (6) and (7) in the range $-k^-<l^-<0$, should be included. However, it is easy to confirm that they are irrelevant to the analysis of the Glauber divergences. An alternative demonstration of the existence of the Glauber divergence in Fig. 2(d) by means of the Feynman parametrization of the corresponding loop integrand is presented in the Appendix.

For Fig. 2(e), the Ward identity is applied to the virtual-gluon propagators,

$$\frac{1}{[(k-k_1)^2+i\epsilon][(k-k_1+l)^2+i\epsilon]} = \left[\frac{1}{(k-k_1)^2+i\epsilon} - \frac{1}{(k-k_1+l)^2+i\epsilon}\right] \times \frac{1}{l^2+2(k-k_1)\cdot l+i\epsilon}. \tag{10}$$

Here we have chosen the sign of the $i\epsilon$ term in the factor outside the square brackets, such that this factor reduces to the eikonal propagator $1/(-l^- + i\epsilon)$, after picking up the pole $l^+ \approx 0 - i\epsilon$. With this choice the first term in the above splitting can be combined with Figs. 2(b) and 2(c) to contribute to the M_2 meson wave function with the piece of the Wilson lines from a coordinate z_2 to plus infinity [40], where z_2 has been labeled in Fig. 1. As explicitly shown in the Appendix, the first term does not involve a Glauber divergence, so it does not break the universality of the M_2 meson wave function. The second piece in Eq. (10) with the color factor $N_c/2$, with N_c being the number of colors, contains the original Glauber divergence of Fig. 2(e). The eikonal approximation for the spectator propagator $1/[(k_1-l)^2+i\epsilon]$ in Fig. 2(f) also gives $1/(-l^- + i\epsilon)$ but with the color factor $-1/(2N_c)$ [39]. The sum of the second piece in Eq. (10) and Fig. 2(f) then leads to the Glauber divergence with the color factor $N_c/2 - 1/(2N_c) = C_F$.

We examine the effects from Fig. 3, which is similar to Fig. 2 but with the collinear gluon being emitted by the valence antiquark of M_2. Figures 3(a)–3(c) do not generate Glauber divergences, and they also contribute to the M_2 meson wave function. For example, the attachment to the b quark in Fig. 3(a) gives rise to the eikonal propagator $1/(l^- + i\epsilon)$ as in Eq. (3), namely, the first piece of the Wilson lines, which runs from minus infinity to the origin. Figure 3(d) contains the four denominators

$$[(k_2+l)^2+i\epsilon][(k+l)^2+i\epsilon][(k-k_1+l)^2+i\epsilon](l^2+i\epsilon), \tag{11}$$

whose corresponding l^+ poles are the same as in Eqs. (5)–(8). Therefore, the allowed range of l^- reduces to $-(P_2^- - k_2^-)<l^-<0$ without the pole in Eq. (9), and this diagram does not contain a Glauber divergence. This observation is also confirmed in the Appendix by means of the Feynman parametrization of the corresponding loop integrand. Figures 2(d) and 3(d) have the same amplitudes in the soft region with $l \sim O(\Lambda_{\rm QCD})$ except for a sign difference, which is attributed to the emissions of the collinear gluon by the valence quark and valence antiquark in M_2. Because of this soft cancellation, the contour of l^- in Fig. 2(d) can be deformed away from the $O(\Lambda_{\rm QCD})$ region, and the eikonalization of the spectator $1/[(k+l)^2+i\epsilon]$ into $1/(l^- + i\epsilon)$ is justified [29]; that is, Fig. 3(d) provides soft subtraction for Fig. 2(d), but it does not remove its Glauber divergence. The

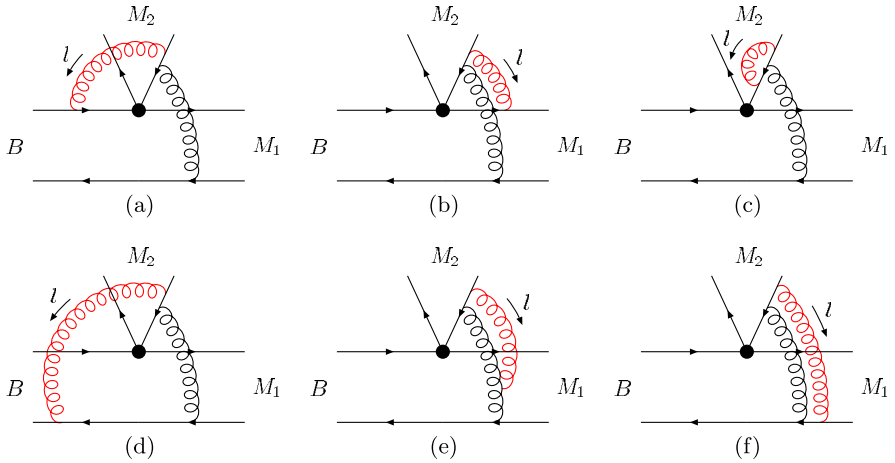

FIG. 3 (color online). More NLO diagrams for Fig. 1(a).

soft cancellation also occurs between Figs. 2(e) and 3(e), and between Figs. 2(f) and 3(f).

The NLO residual infrared divergences in Figs. 2(d)–2(f) are then extracted from the Glauber region,

$$gC_F \int \frac{d^4l}{(2\pi)^4} \mathrm{tr}\Big[\cdots \frac{-i(\not k_2 - \not k + \not k_1 - \not l)}{(k_2 - k + k_1 - l)^2 + i\epsilon} \times (-ig\gamma_\beta)\gamma_5 \not P_2 (-ig\gamma^-) \frac{i(\not P_2 - \not k_2 + \not l)}{(P_2 - k_2 + l)^2 + i\epsilon}\Big] \times \frac{-i}{(k - k_1 + l)^2 + i\epsilon} \frac{-i}{l^2 + i\epsilon} 2\pi i \delta(l^-), \tag{12}$$

where the … denotes the rest of the integrand, and $\gamma_5 \not P_2$ comes from the twist-2 structure of the M_2 meson wave function. The l^+ poles in Eq. (12) are given by Eqs. (5), (7), and (9) with $l^- = 0$ from the valence-quark propagator, the virtual-gluon propagator, and the virtual-quark propagator, respectively. Only the pole in Eq. (5) is of $O(\Lambda^2_{\mathrm{QCD}}/m_B)$. As long as k_1^+ is of or greater than $O(\Lambda_{\mathrm{QCD}})$, we can deform the contour of l^+, such that l^+ remains $O(\Lambda_{\mathrm{QCD}})$, and the hierarchy

$$(P_2^- - k_2^-) l^+ \sim O(m_B \Lambda_{\mathrm{QCD}}) \gg |\mathbf{l}_T - \mathbf{k}_{2T}|^2 \sim O(\Lambda^2_{\mathrm{QCD}}) \tag{13}$$

holds. The valence quark carrying the momentum $P_2 - k_2 + l$ in Eq. (12) can then be eikonalized into $1/(l^+ + i\epsilon)$.

Equation (12) is factorized into

$$g^2 C_F \int \frac{d^4l}{(2\pi)^4} \mathrm{tr}\Big[\cdots \frac{-i(\not k_2 - \not k + \not k_1 - \not l)}{(k_2 - k + k_1 - l)^2 + i\epsilon} (-ig\gamma_\beta)\gamma_5 \not P_2\Big] \times \frac{-i}{(k - k_1 + l)^2 + i\epsilon} \frac{1}{l^+ + i\epsilon} \frac{-i}{l^2 + i\epsilon} 2\pi i \delta(l^-). \tag{14}$$

The above factorization of the Glauber gluon follows exactly the reasoning applied to the low-p_T hadron hadroproduction in Ref. [35]. We close the contour in the lower half plane of l^+, and pick up only the pole $l^+ \approx 0 - i\epsilon$ from the eikonal propagator $1/(l^+ + i\epsilon)$, which corresponds to an on-shell valence-quark propagator. Another pole corresponding to the on-shell right gluon contributes to the Glauber divergence associated with Fig. 1(b) [29]. We then derive explicitly the imaginary logarithm,

$$i\frac{\alpha_s}{\pi} C_F \int \frac{d^2 l_T}{l_T^2} \mathcal{M}_a^{(0)}(\mathbf{l}_T), \tag{15}$$

where $\mathcal{M}_a^{(0)}$ denotes the LO spectator amplitude from Fig. 1(a). The gluon propagator proportional to $1/l_T^2$ indicates that the infrared divergence we have identified arises from the Glauber region.

Below we investigate the Glauber divergences appearing in the NLO corrections to Fig. 1(b), which are associated with the M_2 meson. The relevant diagrams contain the attachments of the collinear gluons emitted by the valence antiquark of M_2 as depicted in Fig. 4. For the attachment to the virtual gluon in Fig. 4(b), we adopt the splitting

$$\frac{1}{[(k - k_1)^2 + i\epsilon][(k - k_1 + l)^2 + i\epsilon]} = \left[\frac{1}{(k - k_1)^2 + i\epsilon} - \frac{1}{(k - k_1 + l)^2 + i\epsilon}\right] \times \frac{1}{l^2 + 2(k - k_1)\cdot l - i\epsilon}, \tag{16}$$

where the second term on the right-hand side contains the Glauber divergence in the original NLO diagram. The first term then contributes to the definition of the M_2 meson wave function. A similar analysis implies that the diagrams in Fig. 4 contain the Glauber divergences

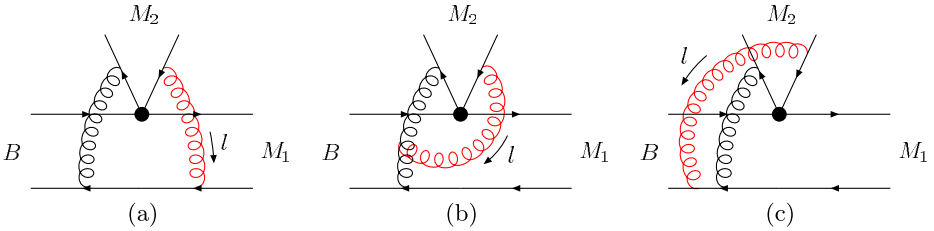

FIG. 4 (color online). NLO diagrams for Fig. 1(b) that contribute to the Glauber divergences associated with the M_2 meson.

$$-i\frac{\alpha_s}{\pi}C_F\int\frac{d^2l_T}{l_T^2}\mathcal{M}_b^{(0)}(\mathbf{l}_T), \tag{17}$$

where $\mathcal{M}_b^{(0)}$ denotes the LO spectator amplitude from Fig. 1(b). The additional minus sign compared to Eq. (15) is attributed to the collinear gluon emission by the valence antiquark of M_2.

It has been shown that the residual infrared divergences appear between the M_2 meson and the $B\to M_1$ transition [29]. It is natural to ask whether there exist more residual infrared divergences in the spectator amplitude of the $B\to M_1M_2$ decay. We shall verify that this is the case: additional Glauber divergences associated with the M_1 meson are induced by the inclusion of the Glauber divergences associated with the M_2 meson. Consider all possible attachments of the collinear gluons emitted by the valence quark of M_1 to particle lines in Fig. 1(a), among which the diagram in Fig. 5(a) contains a Glauber divergence as implied by the pole analysis of the following five denominators:

$$[(P_1-k_1+l)^2+i\epsilon][(k+l)^2+i\epsilon][(k-k_1+l)^2+i\epsilon]\times(l^2+i\epsilon)[(k_2-k+k_1-l)^2+i\epsilon]. \tag{18}$$

Nonvanishing contributions come from the ranges $0<l^+<k_1^+$, $-k^+<l^+<0$, and $-(P_1^+-k_1^+)<l^+<-k^+$, where the poles of l^- are given by

$$l^-\approx\frac{|\mathbf{l}_T-\mathbf{k}_{1T}|^2}{2(l^++P_1^+-k_1^+)}-i\epsilon(-i\epsilon,-i\epsilon), \tag{19}$$

$$l^-=-k^-+\frac{|\mathbf{l}_T+\mathbf{k}_T|^2}{2(l^++k^+)}-i\epsilon(-i\epsilon,+i\epsilon), \tag{20}$$

$$l^-=\frac{l_T^2}{2l^+}-i\epsilon(+i\epsilon,+i\epsilon), \tag{21}$$

$$l^-=-k^-+\frac{|\mathbf{l}_T-\mathbf{k}_{1T}+\mathbf{k}_T|^2}{2(l^+-k_1^+)}+i\epsilon(+i\epsilon,+i\epsilon), \tag{22}$$

$$l^-=k_2^-+\frac{|\mathbf{l}_T-\mathbf{k}_{2T}-\mathbf{k}_{1T}+\mathbf{k}_T|^2}{2(l^+-k_1^+)}+i\epsilon(+i\epsilon,+i\epsilon), \tag{23}$$

respectively. We pick up the first pole $l^-\sim O(\Lambda_{\rm QCD}^2/m_B)-i\epsilon$, which corresponds to the collinear gluon associated with the valence quark of M_1. It is seen that the allowed range for this pole, $-(P_1^+-k_1^+)<l^+<k_1^+$, covers the origin $l^+=0$, leading to a Glauber divergence from the eikonalized spectator propagator $1/(k+l)^2$ and the on-shell radiative gluon.

The residual Glauber divergence in Fig. 5(a) yields the NLO spectator amplitude

$$g\frac{-1}{2N_c}\int\frac{d^4l}{(2\pi)^4}\mathrm{tr}\left[\ldots(-ig\gamma^+)\frac{i(\not P_1-\not k_1+\not l)}{(P_1-k_1+l)^2+i\epsilon}\gamma_\mu\times(1-\gamma_5)\frac{-i(\not k_2-\not k+\not k_1-\not l)}{(k_2-k+k_1-l)^2+i\epsilon}(-ig\gamma_\beta)\gamma_5\not P_2\right]\times\frac{-i}{(k-k_1+l)^2+i\epsilon}\frac{-i}{l^2+i\epsilon}\pi i\delta(l^+). \tag{24}$$

The l^- poles in the above expression are given by Eqs. (19) and (23) with $l^+=0$ from the valence-quark propagator in M_1 and the virtual-quark propagator, respectively. The pole in Eq. (19) is of $O(\Lambda_{\rm QCD}^2/m_B)$, and the pole in Eq. (23) is of $O(m_B)$, so we can deform the contour of l^- such that l^- remains at least $O(\Lambda_{\rm QCD})$, and the hierarchy

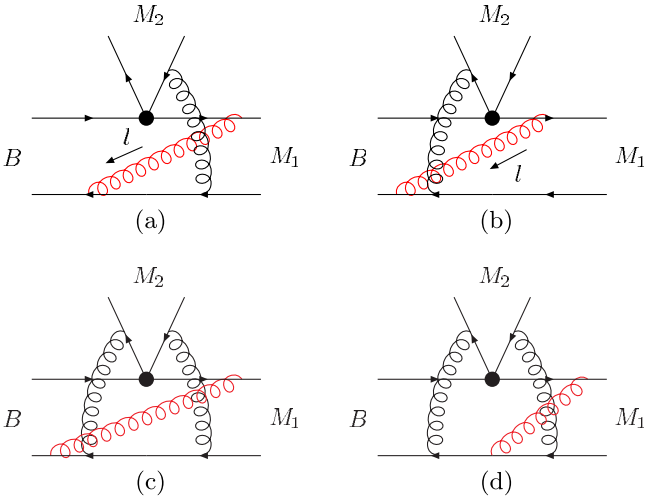

FIG. 5 (color online). (a)–(c) Higher-order corrections to Fig. 1 that contain the Glauber divergences associated with the M_1 meson. (d) Higher-order correction to Fig. 1 that does not contain the Glauber divergence associated with the M_1 meson.

$$(P_1^+ - k_1^+)l^- \sim O(m_B\Lambda_{\rm QCD}) \gg |\mathbf{l}_T - \mathbf{k}_{1T}|^2 \sim O(\Lambda_{\rm QCD}^2) \tag{25}$$

holds. The valence quark carrying the momentum $P_1 - k_1 + l$ is thus eikonalized into $1/(l^- + i\epsilon)$. Equation (24) is factorized into

$$\begin{aligned} & g^2\frac{-1}{2N_c}\int\frac{d^4l}{(2\pi)^4}\mathrm{tr}\left[\ldots\gamma_\mu(1-\gamma_5)\frac{-i(\not k_2 - \not k + \not k_1 - \not l)}{(k_2 - k + k_1 - l)^2 + i\epsilon}\right. \\ & \left.\times(-ig\gamma_\beta)\gamma_5 P_2\right]\frac{-i}{(k - k_1 + l)^2 + i\epsilon} \\ & \times\frac{1}{l^- + i\epsilon}\frac{-i}{l^2 + i\epsilon}\pi i\delta(l^+), \\ & \approx -i\frac{1}{2N_c}\frac{\alpha_s}{2\pi}\int\frac{d^2l_T}{l_T^2}\mathcal{M}_a^{(0)}(\mathbf{l}_T), \end{aligned} \tag{26}$$

where we have closed the contour in the lower half plane of l^- over the pole $l^- \approx 0 - i\epsilon$ from the eikonal propagator $1/(l^- + i\epsilon)$.

Figure 5(b) gives the same Glauber divergence as in Eq. (26), since the collinear gluon is also emitted by the valence quark of M_1 and attaches to the spectator of the B meson:

$$-i\frac{1}{2N_c}\frac{\alpha_s}{2\pi}\int\frac{d^2l_T}{l_T^2}\mathcal{M}_b^{(0)}(\mathbf{l}_T). \tag{27}$$

The Glauber divergences in Eqs. (26) and (27) can also be verified by means of the Feynman parametrization of the loop integrands, as shown in the Appendix. Because of the destruction between the LO amplitudes $\mathcal{M}_a^{(0)}$ and $\mathcal{M}_b^{(0)}$, these Glauber divergences cancel each other. The same cancellation also occurs between the pair of diagrams with the collinear gluons attaching to the virtual gluons in Figs. 1(a) and 1(b). This then implies that there are no additional Glauber divergences at NLO in the $B \to M_1M_2$ decay, except those associated with the M_2 meson. The other collinear gluon emissions from the valence quark and from the spectator of M_1 contribute only to the construction of the M_1 meson wave function, which contains the Wilson lines running from the origin to infinity, and then from infinity to the coordinate z_1 labelled in Fig. 1(a). The cancellation of the soft divergences—similar to that between Figs. 2 and 3—also occurs between the above two sets of diagrams.

Nevertheless, the Glauber divergences associated with the M_1 meson exist at next-to-next-to-leading order. Once the Glauber gluons associated with the M_2 meson are included, the interference between the two spectator amplitudes $\mathcal{M}_a$ and $\mathcal{M}_b$ becomes constructive, and the cancellation between Eqs. (26) and (27) no longer occurs. A corresponding diagram is displayed in Fig. 5(c), in which the two vertical gluon lines contribute to the Glauber divergences for Figs. 1(a) and 1(b), and the third gluon emitted by M_1 gives a common Glauber divergence. The color factor for Fig. 5(c) is given by

$$\begin{aligned} \mathrm{tr}(T^cT^aT^bT^cT^bT^a) = & \frac{1}{2}\mathrm{tr}(T^aT^b)\mathrm{tr}(T^bT^a) \\ & - \frac{1}{2N_c}\mathrm{tr}(T^aT^bT^bT^a), \end{aligned} \tag{28}$$

where T^a, T^b, and T^c are associated with the left vertical gluon, the right vertical gluon, and the third gluon, respectively. The first term in the above expression corresponds to a color flow from the four-fermion operator O_1. Since we focus on the spectator amplitude from O_2 in this work, this contribution will be dropped. The second term corresponds to the color flow of the original spectator amplitude, implying that the color factors for the Glauber divergences associated with the M_2 and M_1 mesons remain as in Eqs. (15), (17), (26), and (27).

It can be shown that the attachments of the third gluon to other lines—for example, to the spectator line between the two vertical gluons in Fig. 5(d)—do not produce Glauber divergences. The reason is explained below. We route the loop momentum of the third gluon through the left-handed vertical gluon. When this left-handed vertical gluon is hard (the right-handed vertical gluon is soft), the third gluon contributes only to the M_1 meson wave function: the diagram can be regarded as a two-particle reducible correction to the M_1 meson wave function with the right-handed vertical soft gluon coupling the M_2 meson and the B-M_1 system; that is, it does not contribute to the Glauber divergence, which breaks the factorization. When the left-handed vertical gluon is soft (the right-handed vertical gluon is hard), the valence quark of the M_2 meson remains on shell and collimated to the M_2 meson. In this case its momentum is independent of k_1, and it does not constrain the contour in the l^- plane. When both vertical gluons are hard, Fig. 5(d) contributes to the NLO hard kernel, which goes beyond the accuracy of the present calculation.

A remark is in order. It has been shown that a Glauber divergence exists in Fig. 2(f), where the radiative gluon of momentum l attaches partons in the M_1 and M_2 mesons. A simple way to tell whether this Glauber divergence is associate with the M_1 or M_2 meson is to investigate the pole structures. By replacing the spectator propagator by $\delta(l^-)$ [as was done in Eq. (12)], we check the pole positions in the complex l^+ plane and find that the l^+ contour for Fig. 2(f) is constrained by the valence-quark propagator and the valence-antiquark propagator of M_2. On the contrary, by replacing the valence-quark propagator of M_2 with $\delta(l^+)$ we see that the l^- contour is not constrained. The above difference in the pole structures of l^+ and l^- implies that the observed Glauber divergence should be associated with the M_2 meson. We then complete the investigation of the

Glauber divergences in the spectator amplitudes for the two-body hadronic B-meson decays. The exponentiation of the NLO results in Eqs. (15) and (17) [29] and in Eqs. (26) and (27) leads to the parametrization

$$M_a^G = \exp(-iS_{e1})\exp(iS_{e2})\mathcal{M}_a^{(0)},$$
$$M_b^G = \exp(-iS_{e1})\exp(-iS_{e2})\mathcal{M}_b^{(0)}, \tag{29}$$

where the signs have followed the indication of the NLO results. It is obvious that the destruction between M_a^G and M_b^G retains, as the Glauber factors associated with the M_2 meson are turned off, i.e., $S_{e2}=0$. Strictly speaking, Eq. (29)—derived while neglecting the dependence on the Glauber gluon transverse momentum—holds only approximately. We shall treat the Glauber phases S_{e1} and S_{e2} as free parameters in the numerical analysis later. A definition for the Glauber factor in terms of a matrix element of four Wilson lines was constructed in Ref. [35].

At last, we point out the connection between the Glauber gluon exchanges and the elastic scattering in two-body hadronic B-meson decays. The analysis of Refs. [33,34] started with the amplitudes evaluated in the QCDF approach, and final-state interaction effects were included via the elastic rescattering. We take only the rescattering between the $B^0\to\pi^+\pi^-$ and $B^0\to\pi^0\pi^0$ modes as an example,

$$\begin{pmatrix}\pi^+ & \pi^-\\ \pi^0 & \pi^0\end{pmatrix} = S_{\rm res}^{1/2}\begin{pmatrix}\pi^+ & \pi^-\\ \pi^0 & \pi^0\end{pmatrix}_{\rm QCDF}, \tag{30}$$

with the matrix $S_{\rm res}^{1/2}\equiv(1+i\mathcal{T})^{1/2}$ parametrizing the rescattering effects. The matrix $\mathcal{T}$ is written as

$$\mathcal{T} = \begin{pmatrix} r_0+2r_a+r_t & (2r_a-r_e+r_t)/\sqrt{2}\\ (2r_a-r_e+r_t)/\sqrt{2} & r_0+(2r_a+r_e+r_t)/2\end{pmatrix}, \tag{31}$$

where the parameters r_0, r_e r_a, and r_t denote the mechanism from the singlet exchange, the charge exchange, the annihilation, and the total annihilation, respectively. The best fit to the $B\to PP$ data gave the following combined parameters defined in Eq. (15) of Ref. [34]:

$$1+i(r_0+r_a) = 0.94+0.58i,$$
$$i(r_e-r_a) = 0.06-0.58i,$$
$$i(r_a+r_t) = -0.12-0.09i, \tag{32}$$

which seem to indicate that the annihilation and the total annihilation are less important, and r_0 and r_e are roughly of the same order of magnitude.

Compared to the above formalism, the standard NLO pQCD decay amplitudes correspond to the inputs on the right-hand side of Eq. (30), and the Glauber gluon exchanges correspond to the matrix $\mathcal{T}$. The Glauber gluons do not generate the annihilation r_a and r_t, an observation consistent with the numerical outcomes in Eq. (32). We elaborate that the amplitude in Eq. (15) contributes to r_0, and that in Eq. (17) contributes to r_e. We insert the identity for the color matrices

$$I_{ij}I_{lk} = \frac{1}{N_c}I_{lj}I_{ik} + 2(T^c)_{lj}(T^c)_{ik} \tag{33}$$

into M_b^G, with I_{ij} (I_{lk}) being the unity matrix associated with the meson M_1 (M_2). The second term in the decomposition, associated with a meson in the color-octet state, will not be considered here. The matrix I_{lj} in the first term implies that the valence quark in M_1 and the valence antiquark in M_2 form a color-singlet state. The matrix I_{ik} implies that the valence antiquark in M_1 and the valence quark in M_2 form a color-singlet state. It is easy to see that the resultant topology corresponds to the color-allowed tree amplitude T. Therefore, M_b^G can be regarded as a contribution from the $B^0\to\pi^+\pi^-$ intermediate state (dominated by the amplitude T) to the $B^0\to\pi^0\pi^0$ decay (dominated by C) through the mechanism of charge exchange. The above color rearrangement does not apply to the amplitude M_a^G, since the color trace of I_{lj} and the color matrix associated with the hard gluon vertex vanishes. Hence, M_a^G represents the contribution from the $B^0\to\pi^0\pi^0$ intermediate state to itself through the singlet exchange. Certainly, the Glauber effect and the elastic rescattering are essentially different. For instance, the former is crucial only in the pion-involved decays, while the latter contributes to all relevant modes under the SU(3) flavor symmetry.

III. NUMERICAL ANALYSIS

As postulated in Ref. [29], the Glauber effect from the multiparton states is more significant in the pion than in other mesons. This postulate can be understood by means of the simultaneous role of the pion as a $q\bar{q}$ bound state and as a NG boson [31]. The valence quark and antiquark of the pion are separated by a short distance in order to reduce the confinement potential energy, while the multiparton states of the pion spread over a huge spacetime in order to meet the role of a massless NG boson; that is, the multiparton states distribute more widely than the $q\bar{q}$ state does in the pion compared to other mesons. This explains the strong Glauber effect from the pion, which will be examined in this section. The standard pQCD factorization formulas for the $B\to\pi\pi$ and πK decays are referred to [26], while those for the $B\to\pi\rho$ and $\pi\omega$ decays [5,6] can be obtained by taking into account the differences between $B\to PP$ and PV modes, as illustrated in Refs. [41,42].

Following Eq. (29), we multiply the b-quark spectator amplitudes in NLO pQCD, both tree and penguin, by $\exp(iS_{e2})$ [$\exp(-iS_{e2})$] with the hard gluon being emitted

by the valence antiquark (quark) in M_2, if M_2 denotes a pion. We also multiply the above spectator amplitudes by $\exp(-iS_{e1})$ if M_1 denotes a pion. As mentioned in Ref. [26], the color-suppressed tree amplitude in the $B \to \pi\pi$ decays is small at LO due to the small Wilson coefficient a_2 for the factorizable contribution and to the cancellation between Figs. 1(a) and 1(b) for the spectator contribution. The presence of the Glauber factor $\exp(\pm iS_{e2})$ converts the destructive interference in Fig. 1 into a constructive one, resulting in strong enhancement. The Glauber factor $\exp(-iS_{e1})$ further rotates the enhanced spectator amplitude and modifies its interference with other emission amplitudes. This effect will adjust the relative phase between the color-allowed and color-suppressed tree amplitudes, such that all three $B \to \pi\pi$ branching ratios are accommodated at the same time.

The choices of the distribution amplitudes for the B meson, pseudoscalar mesons, and vector mesons are the same as in Ref. [41], but with the updated values of the meson decay constants: $f_B = 191$ MeV, $f_\pi = 130$ MeV, $f_K = 156$ MeV, $f_\rho = 216$ MeV, $f_\rho^T = 165$ MeV, $f_\omega = 187$ MeV, and $f_\omega^T = 151$ MeV [43,44]. We also update the meson masses $m_B = 5.28$ GeV, $m_\pi = 0.137$ GeV, $m_K = 0.495$ GeV, $m_\rho = 0.77$ GeV, and $m_\omega = 0.783$ GeV, the quark masses $m_q = 6.5$ MeV, $m_s = 140$ MeV, $m_c = 1.5$ GeV, and $m_b = 4.8$ GeV (which appear in the quark-loop and magnetic-penguin amplitudes), the chiral scales $m_{0\pi} = 1.6$ GeV and $m_{0K} = 1.8$ GeV, the B-meson lifetimes $\tau_{B^0} = 1.519 \times 10^{-12}$ s and $\tau_{B^\pm} = 1.641 \times 10^{-12}$ s, the Cabibbo-Kobayashi-Maskawa matrix elements $V_{ud} = 0.97427$, $V_{us} = 0.22534$, $|V_{ub}| = 3.51 \times 10^{-3}$, $V_{cd} = -0.22520$, $V_{cs} = 0.97344$, and $V_{cb} = 0.0412$, and the weak phases $\phi_1 = 21.5^\circ$ and $\phi_3 = 70^\circ$ [1,43], while the other parameters are taken to be the same as in Ref. [41]. We employ the NLO Wilson coefficients for the emission amplitudes, and the LO ones for the annihilation amplitudes, since the NLO corrections to the weak vertices in the latter are not yet available. The resultant $B \to \pi, K, \rho, \omega$ transition form factors are then given by

$$F_0^{B\pi}(0) = 0.28, \qquad F_0^{BK}(0) = 0.39,$$
$$A_0^{B\rho}(0) = 0.29, \qquad A_0^{B\omega}(0) = 0.27 \tag{34}$$

at maximal recoil, close to those obtained in Ref. [45].

The S_{e1} and S_{e2} dependencies of the color-suppressed tree amplitude C, the color-allowed tree amplitude T, and their ratio for the $B \to \pi\pi$ decays are displayed in Fig. 6, where the definitions of C and T are the same as in Ref. [26]. As argued before, the destructive interference between Figs. 1(a) and 1(b) is moderated by the Glauber factor, so their net contribution increases for nonvanishing S_{e2}. It is observed in Fig. 6 that the magnitude of C reaches a maximum as $S_{e2} \approx -\pi/2$. On the other hand, Figs. 1(a) and 1(b) acquire the same phase factor $\exp(-iS_{e1})$ from the Glauber gluons in the M_1 meson. Despite being an overall factor, it changes the relative phase between the spectator amplitude and the factorizable emission amplitude, which includes the important vertex corrections at NLO [26]. Therefore, C also depends on S_{e1}, whose magnitude reaches a maximum for $S_{e1} \approx S_{e2} \approx -\pi/2$. Because T receives contributions from both the factorizable and spectator diagrams, the Glauber factors affect its magnitude and argument. Due to the dominance of the former

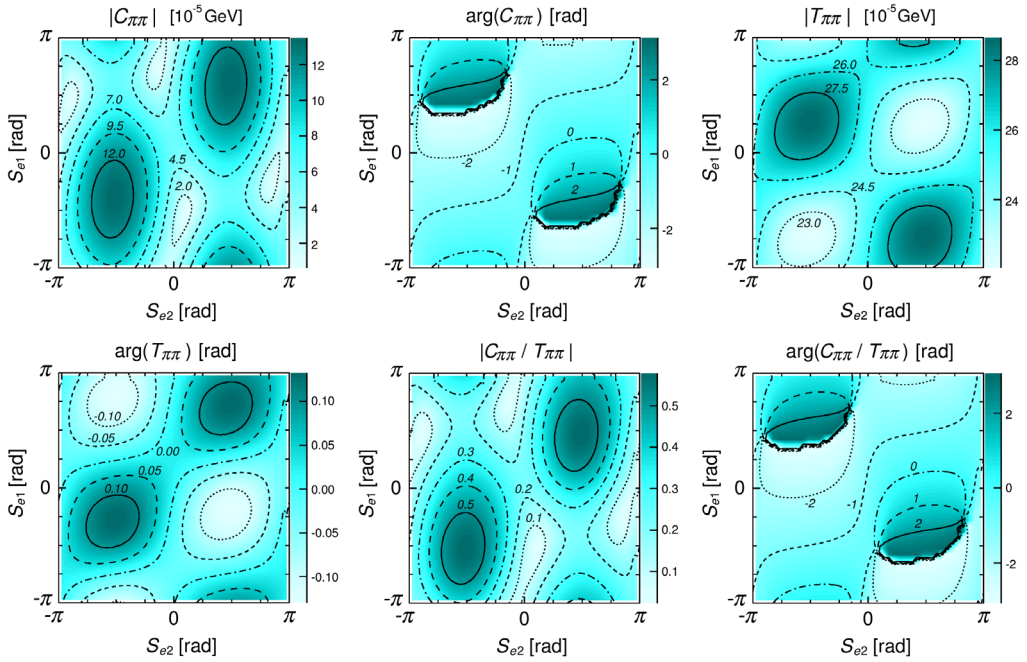

FIG. 6 (color online). S_{e1} and S_{e2} dependencies of the amplitudes C and T, and their ratio C/T for the $B \to \pi\pi$ decays.

contribution, the Glauber effect on T is minor compared to the effect on C. Figure 6 shows that the magnitude of the amplitude ratio C/T is enhanced by a factor of 3 as $S_{e1} \approx S_{e2} \approx -\pi/2$, relative to the value at $S_{e1} = S_{e2} = 0$. The result $C/T = 0.58e^{-0.9i}$ at $S_{e1} = S_{e2} = -\pi/2$ for the $B \to \pi\pi$ decays is close to the extraction in Ref. [2].

Similar plots for the $B \to \pi\rho$ and πK decays are displayed in Fig. 7. The plots for the $B \to \pi\omega$ decays, similar to those for the $B \to \pi\rho$ ones, are not presented here. Since only a single pion is involved in each mode, either the Glauber phase S_{e1} or S_{e2} appears in the modified pQCD factorization formula. For those modes containing the $B \to \pi$ transition, the corresponding amplitude ratio $C_{\pi\rho}/T_{\pi\rho}$ depends on S_{e1} only: the magnitude of $C_{\pi\rho}/T_{\pi\rho}$ decreases by about 40%, and the argument decreases by about 10% as S_{e1} varies from zero to $-\pi/2$. For those modes with $M_2 = \pi$, the corresponding amplitude ratios $C_{\rho\pi}/T_{\rho\pi}$ and $C_{K\pi}/T_{\pi K}$ mainly depend on S_{e2}: both the magnitude and argument increase by a factor of 2 as S_{e2} varies from zero to $-\pi/2$. As explained before, the variation of S_{e2} modifies the interference pattern between the two spectator diagrams in Fig. 1, such that the corresponding Glauber effect always enhances the magnitude of C/T. Compared to the $B \to \pi\pi$ case, the Glauber effects are minor in the $B \to \pi\rho$, $\pi\omega$, and πK decays, as expected.

The S_{e1} and S_{e2} dependencies of the $B \to \pi\pi$ branching ratios (in units of 10^{-6}) and direct CP asymmetries are shown in Fig. 8. It is found that the combined effect from the two Glauber factors decreases the $B^0 \to \pi^+\pi^-$ branching ratio from 7.5×10^{-6} (corresponding to $S_{e1} = S_{e2} = 0$) to 6.4×10^{-6} (corresponding to $S_{e1} = S_{e2} = -\pi/2$). On the contrary, the $B^+ \to \pi^+\pi^0$ branching ratio increases from 5.0×10^{-6} to 6.6×10^{-6}; that is, the ratio of the above two predictions becomes consistent with the data. The Glauber effect is not dramatic, because these two modes are dominated by the color-allowed tree amplitude T. The enhancement of the $B^0 \to \pi^0\pi^0$ branching ratio from about 0.38×10^{-6} to 1.2×10^{-6} is significant, giving a NLO pQCD prediction that agrees well with the data, $(1.17 \pm 0.13) \times 10^{-6}$. Note that the above data have been updated by combining the *BABAR* data in Ref. [1] with those recently reported by Belle [32]. The improved consistency of the three predicted branching ratios with the data is highly nontrivial, which requires the simultaneous adjustment of the relative phases between the spectator diagrams, and between the spectator amplitude and other emission amplitudes. It is seen that the Glauber factor does not change much the direct CP asymmetries in the $B^0 \to \pi^+\pi^-$ and $B^+ \to \pi^+\pi^0$ decays, which contain the amplitude T. The impact on the $B^0 \to \pi^0\pi^0$ direct CP asymmetry is obvious in Fig. 6: the predicted $A_{CP}(\pi^0\pi^0)$ decreases from 0.59 to 0.36, closer to the central value of the data 0.03 ± 0.17, when one varies the phases from $S_{e1} = S_{e2} = 0$ to $S_{e1} = S_{e2} = -\pi/2$. The above data have been also updated by combining the *BABAR* ones in [1] with those recently reported by Belle [32].

The NLO pQCD predictions for the mixing-induced CP asymmetries in the $B \to \pi\pi$ decays with the variation of S_{e1}

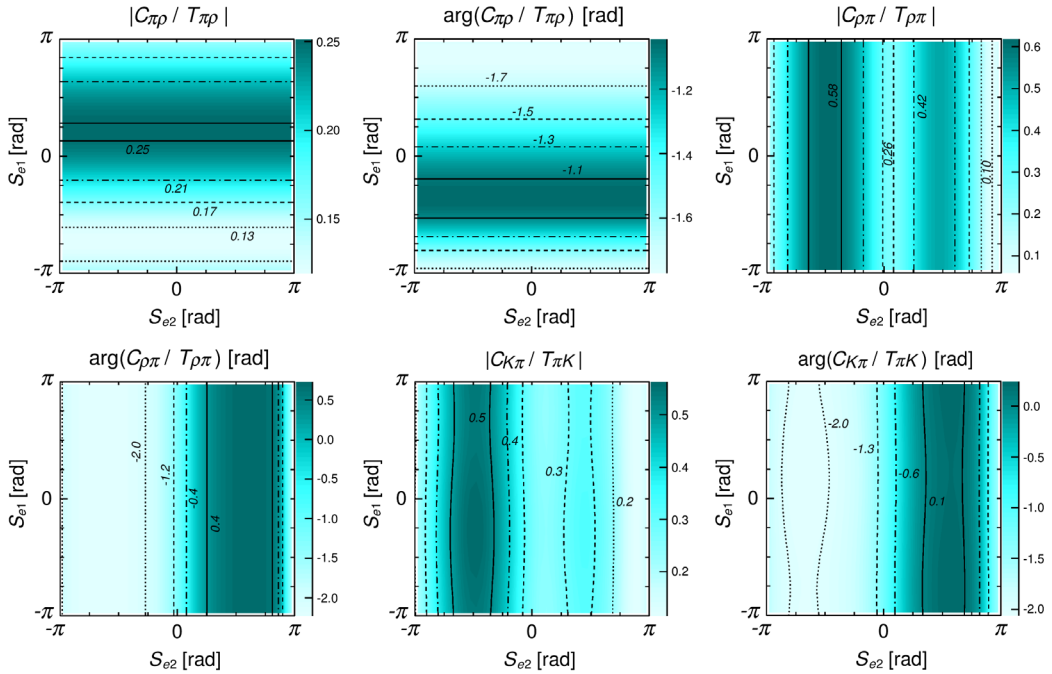

FIG. 7 (color online). S_{e1} and S_{e2} dependencies of the amplitudes C and T, and their ratio C/T for the $B \to \pi\rho$ and πK decays.

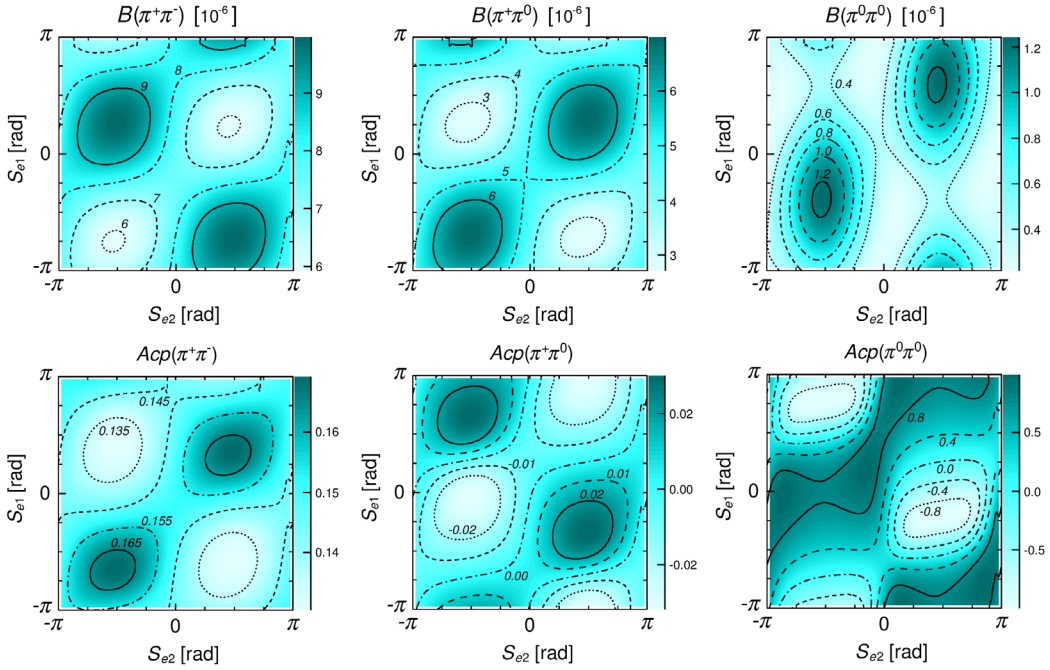

FIG. 8 (color online). S_{e1} and S_{e2} dependencies of the $B \to \pi\pi$ branching ratios (in units of 10^{-6}) and direct CP asymmetries.

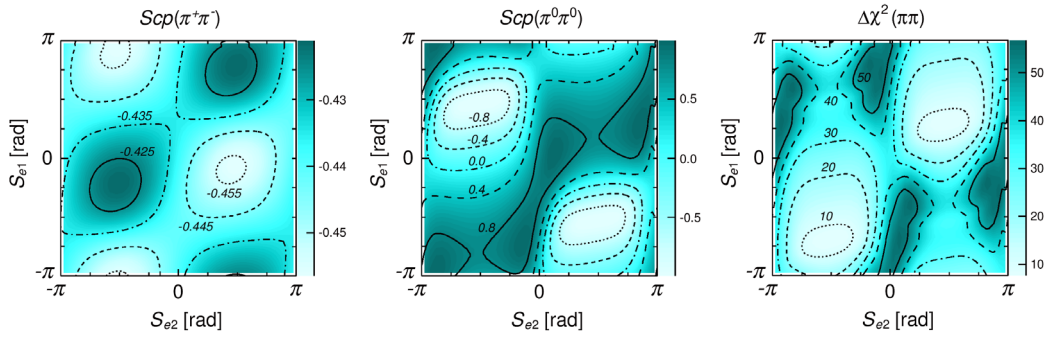

FIG. 9 (color online). S_{e1} and S_{e2} dependencies of the $B \to \pi\pi$ mixing-induced CP asymmetries, and $\Delta\chi^2$.

and S_{e2} are exhibited in Fig. 9. The prediction for $S_{CP}(\pi^0\pi^0)$ is more sensitive to the Glauber phases compared to that for $S_{CP}(\pi^+\pi^-)$, since the $B^0 \to \pi^+\pi^-$ mode is dominated by the color-allowed tree amplitude. The latter remains around -0.43 under the variation of S_{e1} and S_{e2}, which is lower than the data -0.66 ± 0.06 [1]. The former reduces from 0.80 to 0.63 as one tunes the phases from $S_{e1} = S_{e2} = 0$ to $S_{e1} = S_{e2} = -\pi/2$. To quantize the improvement of the consistency between the pQCD predictions and the data attributed to the inclusion of the Glauber phases, we define

$$\Delta\chi^2 = \frac{(\text{data mean} - \text{theory value})^2}{\sqrt{\text{data error}^2 + (0.30 \times \text{theoty value})^2}}, \qquad (35)$$

where the unknown theoretical uncertainty is assumed to be 30%. We stress that we have not attempted to undertake the best fit, but rather to illustrate the improvement by computing $\Delta\chi^2$. The last plot in Fig. 9 summarizes the reduction of $\Delta\chi^2$ in the global fit of the pQCD predictions with the Glauber phases to the $B \to \pi\pi$ data. As expected, the value drops significantly from about 36 (corresponding to $S_{e1} = S_{e2} = 0$) to around 11 (corresponding to $S_{e1} = S_{e2} = -\pi/2$); that is, the Glauber gluons indeed affect the ratio C/T toward the indication of the data.

The S_{e1} and S_{e2} dependencies of the $B \to \pi\rho$ branching ratios (in units of 10^{-6}) and direct CP asymmetries are shown in Fig. 10. Because only a single pion is involved in these modes, the Glauber effect is minor. The NLO pQCD prediction for the branching ratio $B(\pi^\pm\rho^\mp)$ increases a bit from 27.8×10^{-6} to 30.8×10^{-6} as one tunes the phases from $S_{e1} = S_{e2} = 0$ to $S_{e1} = S_{e2} = -\pi/2$, which slightly overshoots the data. The predicted $B(\pi^+\rho^0)$ increases from 6.5×10^{-6} to 7.2×10^{-6}, while the predicted $B(\pi^0\rho^+)$ decreases from 13.3×10^{-6} to 9.3×10^{-6}. The predicted

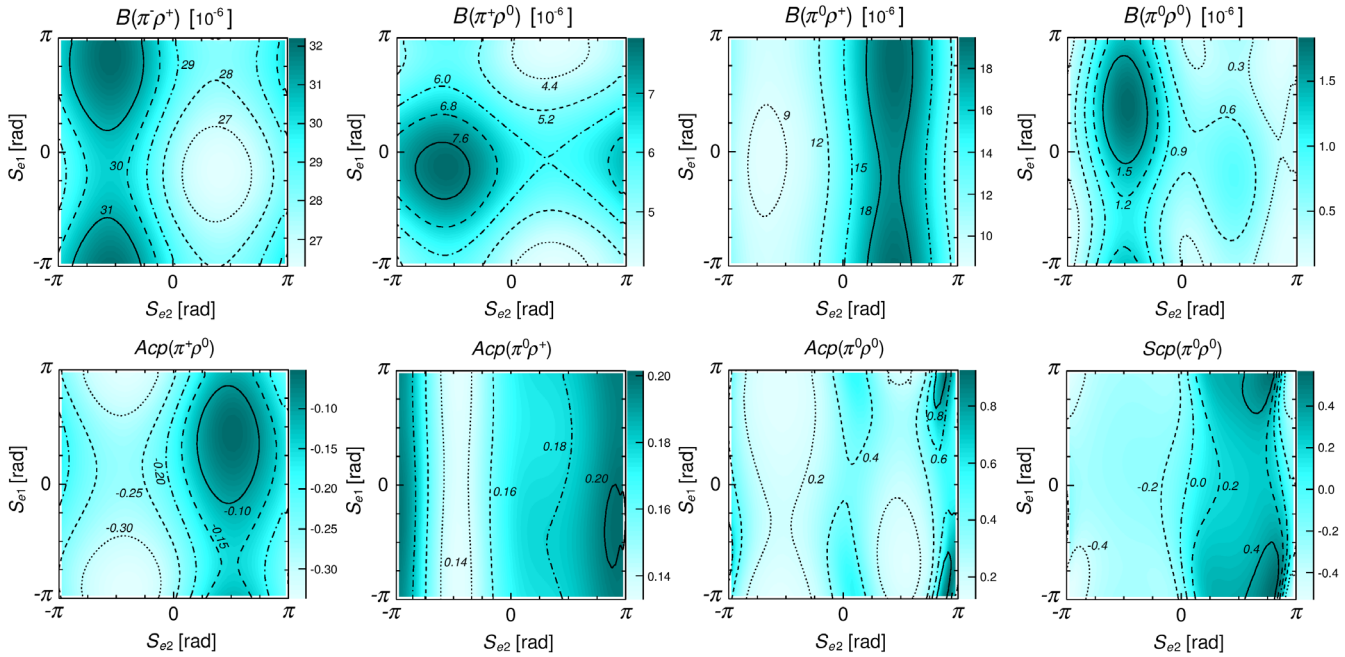

FIG. 10 (color online). S_{e1} and S_{e2} dependencies of the $B \to \pi\rho$ branching ratios (in units of 10^{-6}), direct CP asymmetries, and mixing-induced CP asymmetry.

$B(\pi^0\rho^0)$ changes more dramatically under the variation of the Glauber factors, since it is dominated by the color-suppressed tree amplitude: it is enhanced from 0.70×10^{-6} to about 1.1×10^{-6}. The predictions for $B(\pi^+\rho^0)$ and $B(\pi^0\rho^0)$ become closer to the data. The current data for the direct CP asymmetries in the $B \to \pi\rho$ decays and for the mixing-induced CP asymmetry $S_{CP}(\pi^0\rho^0)$ still suffer huge uncertainties.

The behavior of the $B \to \pi\omega$ modes with the Glauber phases is similar to that of the corresponding $B \to \pi\rho$ modes, as shown in Fig. 11. The NLO pQCD prediction for $B(\pi^+\omega)$ increases from 5.4×10^{-6} to 6.1×10^{-6} as one

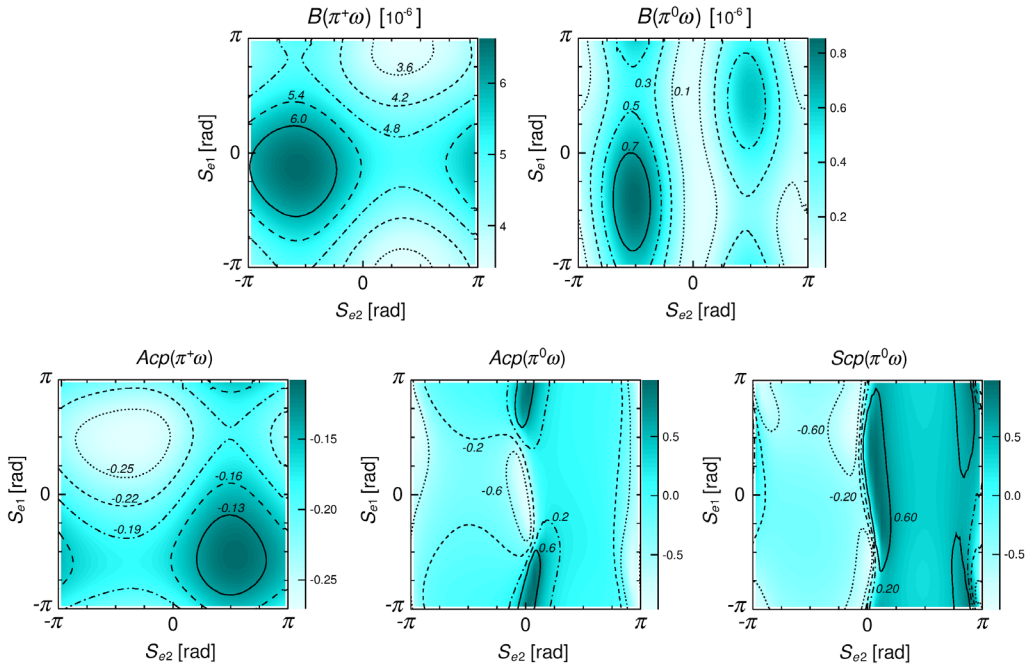

FIG. 11 (color online). S_{e1} and S_{e2} dependencies of the $B \to \pi\omega$ branching ratios (in units of 10^{-6}), direct CP asymmetries, and mixing-induced CP asymmetry.

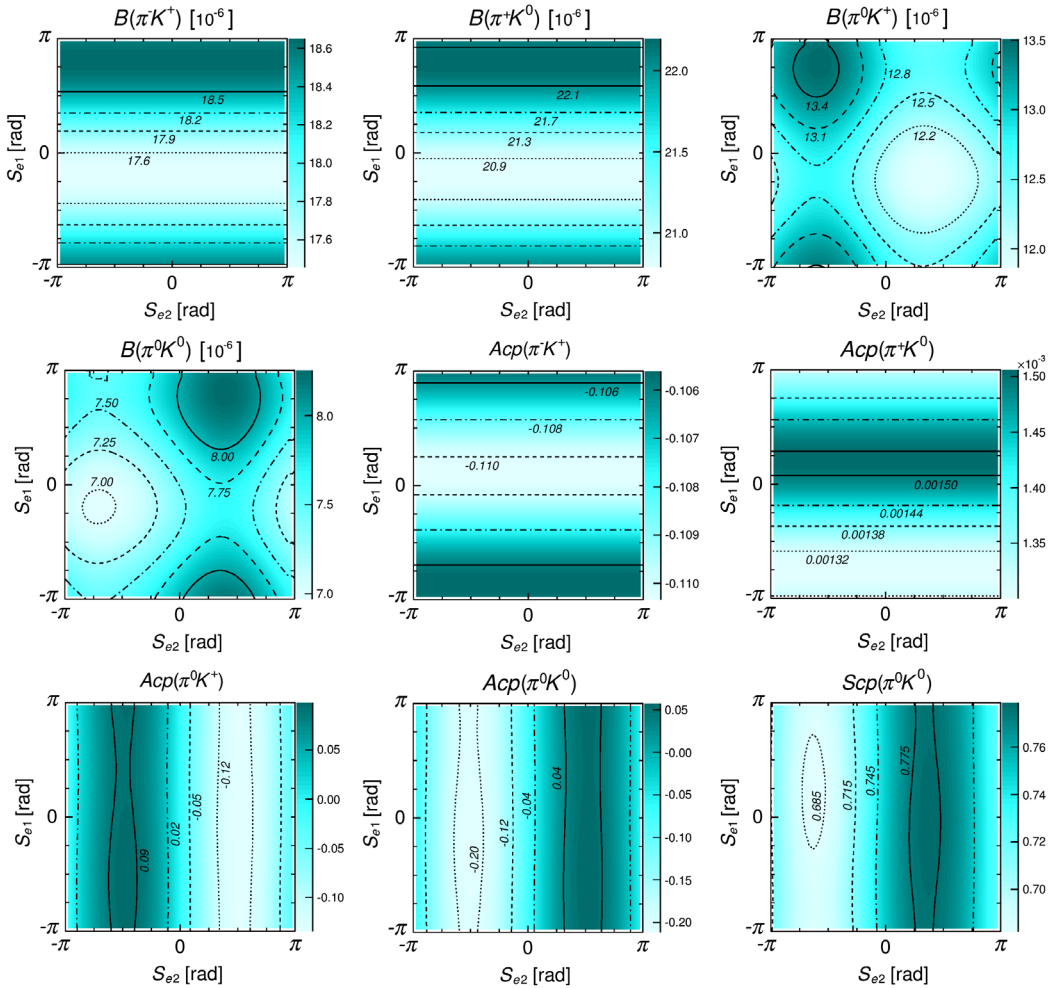

FIG. 12 (color online). S_{e1} and S_{e2} dependencies of the $B \to \pi K$ branching ratios (in units of 10^{-6}), direct CP asymmetries, and mixing-induced CP asymmetry.

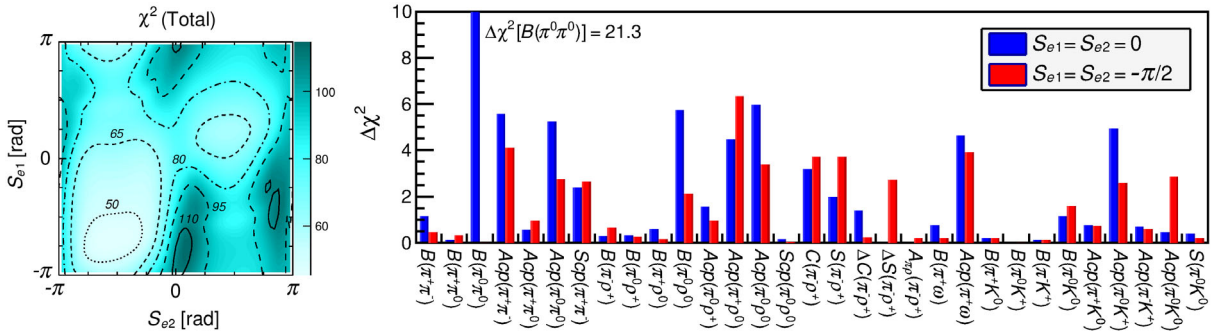

FIG. 13 (color online). S_{e1} and S_{e2} dependencies of $\Delta\chi^2$ for all the $B \to \pi\pi$, $\pi\rho$, $\pi\omega$, and πK decays. The difference of $\Delta\chi^2$ for each considered quantity due to the inclusion of the Glauber effects is also displayed.

tunes the phases from $S_{e1} = S_{e2} = 0$ to $S_{e1} = S_{e2} = -\pi/2$. The modified result is more consistent with the data, $(6.9 \pm 0.5) \times 10^{-6}$ [1]. The prediction for $B(\pi^0\omega)$ increases from 0.04×10^{-6} to 0.85×10^{-6} above the upper bound 0.5×10^{-6} [1]. As remarked before, the present formalism is a simplified one that neglects the convolution between the Glauber factors and the standard pQCD factorization formulas. We shall refine our predictions when the data for $B(\pi^0\omega)$ become available. As for the direct CP asymmetries, the predicted $A_{CP}(\pi^+\omega)$ remains around -0.2 under the variation of the Glauber phases. The CP asymmetries $A_{CP}(\pi^0\omega)$ and $S_{CP}(\pi^0\omega)$ are more sensitive to

TABLE I. Branching ratios (in units of 10^{-6}) and direct CP asymmetries, with the notation $S_e \equiv S_{e1} = S_{e2}$.

	Data [1,32]	$S_e = 0$	$S_e = -\pi/2$		Data [1,32]	$S_e = 0$	$S_e = -\pi/2$
$B(B^0 \to \pi^\mp\pi^\pm)$	5.10 ± 0.19	7.5	6.4	$A_{CP}(B^0 \to \pi^\mp\pi^\pm)$	0.31 ± 0.05	0.15	0.17
$B(B^\pm \to \pi^\pm\pi^0)$	$5.48^{+0.35}_{-0.34}$	5.0	6.6	$A_{CP}(B^\pm \to \pi^\pm\pi^0)$	0.026 ± 0.039	−0.003	−0.012
$B(B^0 \to \pi^0\pi^0)$	1.17 ± 0.13	0.38	1.2	$A_{CP}(B^0 \to \pi^0\pi^0)$	0.03 ± 0.17	0.59	0.36
$B(B^0 \to \pi^\mp\rho^\pm)$	23.0 ± 2.3	27.8	30.8				
$B(B^\pm \to \pi^0\rho^\pm)$	$10.9^{+1.4}_{-1.5}$	13.3	9.3	$A_{CP}(B^\pm \to \pi^0\rho^\pm)$	0.02 ± 0.11	0.17	0.13
$B(B^\pm \to \pi^\pm\rho^0)$	$8.3^{+1.2}_{-1.3}$	6.5	7.2	$A_{CP}(B^\pm \to \pi^\pm\rho^0)$	$0.18^{+0.09}_{-0.17}$	−0.20	−0.31
$B(B^0 \to \pi^0\rho^0)$	2.0 ± 0.5	0.70	1.1	$A_{CP}(B^0 \to \pi^0\rho^0)$	-0.27 ± 0.24	0.38	0.18
$B(B^\pm \to \pi^\pm\omega)$	6.9 ± 0.5	5.4	6.1	$A_{CP}(B^\pm \to \pi^\pm\omega)$	-0.02 ± 0.06	−0.20	−0.18
$B(B^0 \to \pi^0\omega)$	< 0.5	0.04	0.85	$A_{CP}(B^0 \to \pi^0\omega)$	——	−0.99	−0.12
$B(B^\pm \to \pi^\pm K^0)$	23.79 ± 0.75	20.9	21.1	$A_{CP}(B^\pm \to \pi^\pm K^0)$	-0.015 ± 0.019	0.001	0.001
$B(B^\pm \to \pi^0 K^\pm)$	$12.94^{+0.52}_{-0.51}$	12.2	12.9	$A_{CP}(B^\pm \to \pi^0 K^\pm)$	0.040 ± 0.021	−0.01	0.10
$B(B^0 \to \pi^\mp K^\pm)$	$19.57^{+0.53}_{-0.52}$	17.6	17.7	$A_{CP}(B^0 \to \pi^\mp K^\pm)$	-0.082 ± 0.006	−0.11	−0.11
$B(B^0 \to \pi^0 K^0)$	9.93 ± 0.49	7.5	7.2	$A_{CP}(B^0 \to \pi^0 K^0)$	-0.01 ± 0.10	−0.08	−0.21

TABLE II. Mixing-induced CP asymmetries.

	Data [1]	$S_e = 0$	$S_e = -\pi/2$		Data [1]	$S_e = 0$	$S_e = -\pi/2$
$S_{CP}(B^0 \to \pi^\mp\pi^\pm)$	-0.66 ± 0.06	−0.44	−0.43	$S_{CP}(B^0 \to \pi^0\pi^0)$	——	0.80	0.63
$S_{CP}(B^0 \to \pi^0\rho^0)$	-0.23 ± 0.34	−0.09	−0.30	$S_{CP}(B^0 \to \pi^0\omega)$	——	−0.11	−0.26
$S_{CP}(B^0 \to \pi^0 K^0)$	0.57 ± 0.17	0.75	0.69				

TABLE III. CP-violation parameters for the $B^0 \to \pi^\mp\rho^\pm$ decays.

	Data [1]	$S_e = 0$	$S_e = -\pi/2$		Data [1]	$S_e = 0$	$S_e = -\pi/2$
C	-0.03 ± 0.06	0.09	0.10	ΔC	0.27 ± 0.06	0.44	0.32
S	0.06 ± 0.07	−0.04	−0.08	ΔS	0.01 ± 0.08	0.004	−0.14
$\mathcal{A}_{\pi\rho}$	-0.11 ± 0.03	−0.11	−0.13				

the Glauber phases, and the predicted value for the former (latter) varies from −0.99 to −0.12 (from −0.11 to −0.26). The current data for the direct CP asymmetries and mixing-induced CP asymmetry either have large uncertainties or are not yet available.

The S_{e1} and S_{e2} dependencies of the $B \to \pi K$ branching ratios (in units of 10^{-6}), direct CP asymmetries, and mixing-induced CP asymmetry are displayed in Fig. 12. It is easy to understand that the pQCD predictions for all the branching ratios weakly depend on the Glauber phases. $B(\pi^-K^+)$ and $B(\pi^+K^0)$ are insensitive to the variation of S_{e2}, since these two modes do not involve the color-suppressed tree amplitude. The weak dependence on S_{e1} is introduced through the interference between the spectator diagrams and the factorizable emission diagrams. $B(\pi^0K^+)$ and $B(\pi^0K^0)$ depend on both Glauber phases because of the involvement of the color-suppressed tree amplitude. For a similar reason, the direct CP asymmetries $A_{CP}(\pi^-K^+)$ and $A_{CP}(\pi^+K^0)$ are insensitive to the variation of S_{e2}, and slightly depend on S_{e1}. The prediction for $A_{CP}(\pi^-K^+)$ remains as −0.11 while varying S_{e1}, which is close to the data, -0.082 ± 0.006 [1]. On the contrary, $A_{CP}(\pi^0K^+)$ and $A_{CP}(\pi^0K^0)$ depend on S_{e2}, but they are not sensitive to S_{e1}. Note that the amplitude C contains the $B \to K$ transition in this case, and the Glauber effect from the kaon is assumed to be negligible. The predicted $A_{CP}(\pi^0K^+)$ increases from −0.01, and becomes positive quickly as S_{e2} approaches $-\pi/2$, a tendency in agreement with the updated data 0.040 ± 0.021 [1]. The prediction for $A_{CP}(\pi^0K^0)$ decreases from −0.08 to −0.21. This difference is attributed to the sign change of C between the above two modes. Figure 12 indicates that the mixing-induced CP asymmetry $S_{CP}(\pi^0K^0)$ descends from 0.75 to 0.69. Compared to the data $S_{CP}(\pi^0K^0) = 0.57 \pm 0.17$ and $S_{CP}(c\bar{c}s) = 0.682 \pm 0.019$ [1], the consistency has been improved.

At last, we display the S_{e1} and S_{e2} dependencies of $\Delta\chi^2$ for the fit to all the $B \to \pi\pi$, $\pi\rho$, $\pi\omega$, and πK data in Fig. 13,

which exhibits a significant decrease of $\Delta\chi^2$ from 76 to 49, as both S_{e1} and S_{e2} change from zero to $-\pi/2$. Figure 13 also shows the change of $\Delta\chi^2$ for each mode caused by $S_{e1} = S_{e2} = -\pi/2$. The major reduction of $\Delta\chi^2$ arises from the modified predictions for the $B \to \pi\pi$ decays, especially from the $B^0 \to \pi^0\pi^0$ branching ratio. The amount of reduction of $\Delta\chi^2$ from the $B \to \pi\rho$, $\pi\omega$, and πK modes is minor. To summarize the Glauber effects on the quantities considered above, we present the branching ratios and direct CP asymmetries from the data, the standard NLO pQCD predictions with $S_e = S_{e1} = S_{e2} = 0$, and the modified predictions with $S_e = -\pi/2$ in Table I. Those for the mixing-induced CP asymmetries are listed in Table II. Finally, we compute the CP-violation parameters C, ΔC, S, ΔS, and $A_{\pi\rho}$ associated with the $B^0 \to \pi^\mp\rho^\pm$ decays, which were defined in Ref. [1], and present the results in Table III. Our predictions for these observables can be confronted with future data.

IV. CONCLUSION

In this paper we have identified the uncancelled Glauber divergences in the k_T factorization theorem for the spectator amplitudes in the $B \to M_1M_2$ decays at the NLO level. It has been shown that the divergences are factorizable and demand the introduction of the phase factors: those coupling the M_1 meson and the B-M_2 system are absorbed into the phase factor $\exp(-iS_{e1})$, and those coupling the M_2 meson and the $B \to M_1$ transition are absorbed into $\exp(\pm iS_{e2})$. We have investigated the Glauber effects on the color-suppressed tree amplitude C and the color-allowed tree amplitude T in a simplified formalism, in which the convolution between the Glauber factors and the standard pQCD factorization formulas is neglected. Treating S_{e1} and S_{e2} as free parameters, it was observed that the ratio C/T is enhanced maximally by a factor of 3, and a good fit of the pQCD predictions to all the considered $B \to \pi\pi$, $\pi\rho$, $\pi\omega$, and πK data is achieved as $S_{e1} = S_{e2} \approx -\pi/2$.

We summarize the modified NLO pQCD predictions as follows: $B(\pi^0\pi^0)$ and $B(\pi^0\rho^0)$ are increased, the difference between $A_{CP}(\pi^\mp K^\pm)$ and $A_{CP}(\pi^0 K^\pm)$ is enlarged, and $\Delta S_{\pi^0 K_S}$ is reduced, all becoming more consistent with the data. The major reduction of $\Delta\chi^2$ in the global fit arises from the observables for the $B \to \pi\pi$ modes. We stress again that the above improvement is nontrivial, since the simultaneous adjustment of the phases between the spectator diagrams and between the spectator amplitude and other emission amplitudes for these modes is required. The constraint on C from the $B \to \rho\rho$ data is avoided because of the special role of the pion as a $q\bar{q}$ bound state and a pseudo-NG boson. It seems that the implication for new physics from the $B \to \pi K$ puzzle tends to be weaker [46,47].

The Glauber gluons may have a nonperturbative origin similar to that in elastic rescattering. The correspondence has been made explicit between the Glauber factors and the mechanism in elastic rescattering among various M_1M_2 final states, including the singlet exchange and the charge exchange [33,34]. A derivation of the Glauber factor, or even an evaluation of the parameters S_{e1} and S_{e2} by nonperturbative methods for various mesons will lead to a deeper understanding of the proposed mechanism. Besides, the Glauber gluons in the nonfactorizable annihilation amplitudes—which couple the B meson and the M_1-M_2 system—deserves a thorough investigation as well. The inclusion of these additional Glauber gluons will complete the modified pQCD formalism for nonfactorizable $B \to M_1M_2$ decay amplitudes. The above subjects will be studied in forthcoming papers.

We expect that the Glauber effect also appears in other complicated pion-induced processes, if it is really the mechanism responsible for the $B \to \pi\pi$ and πK puzzles. It has been demonstrated recently [48] that the existence of Glauber gluons in the k_T factorization theorem can account for the violation of the Lam-Tung relation [49], namely, the anomalous lepton angular distribution observed in pion-induced Drell-Yan processes [50–52]. It was noticed that a final-state parton is required to balance the lepton-pair transverse momentum q_T, so at least three partons are involved. Since the low-q_T spectra of the lepton pair are involved, the k_T factorization is an appropriate theoretical framework. The Glauber gluons then exist and are factorizable at low q_T, a kinematic region similar to the small-x one for the $B \to \pi\pi$ and πK decays. Associating the Glauber phase factor $\exp(iS_e)$ to the t-channel diagrams, it has been shown that the spin-transverse-momentum correlation between colliding partons—which is necessary for the violation of the Lam-Tung relation—can be generated. More interestingly, this resolution can be discriminated by measuring the $p\bar{p}$ Drell-Yan process at GSI and J-PARC [48].

ACKNOWLEDGMENTS

We thank C. K. Chua and T. Onogi for useful discussions. This work was supported in part by Ministry of Science and Technology of R.O.C. under Grant No. NSC-101-2112-M-001-006-MY3, by the National Center for Theoretical Sciences of R.O.C., by ERC Ideas Advanced Grant no. 267985 "DaMeSyFla," and by ERC Ideas Starting Grant no. 279972 "NPFlavour."

APPENDIX: GLAUBER DIVERGENCES IN FEYNMAN PARAMETRIZATION

In this appendix we verify the existence of the Glauber divergences in the NLO spectator diagrams by means of the Feynman parametrization. Starting with the integrand in Eq. (4) for Fig. 2(d), we associate the Feynman parameters x, t, z, $1-x-y-z-t$, and y with each of the denominators in sequence, obtaining a factor $1/(q^2+2M^2)^5$, with

$$q = l + x(P_2 - k_2) + tk + z(k - k_1) - y(k_2 - k + k_1),$$
$$M^2 = x(y+z)k_1 \cdot (P_2 - k_2) + y(1-y-z) \times k_1 \cdot k_2 - (1-y-z-t)(y+z)k_1 \cdot k. \quad \text{(A1)}$$

Note that the Wick rotation for the variable change $q^0 \to iq^0$ holds, no matter whether M^2 is positive or negative. The two poles of q^0 are always located in the second and fourth quadrants. The difference is that the two poles are closer to the imaginary axis of the q^0 plane when $M^2 > 0$, and to the real axis when $M^2 < 0$. After integrating out q, we arrive at a power of $1/(2M^2 + i\epsilon)$. To get infrared divergences, some of the Feynman parameters need to be small, such that we have small M^2. For example, the collinear divergence from the loop momentum l parallel to P_2 corresponds to $x \sim O(1)$ because $(P_2 - k_2 + l)^2$ is small already, and y, z, and t are all small because their associated denominators are large. A more solid argument on the relations between the Feynman parameters and the presence of infrared singularities can be made with the Landau equations [53].

The sign change of M^2 in the last integral is required for the existence of the Glauber divergences, such that the principal-value prescription applies. We first integrate out x and get a power of $1/(y+z)$ as a coefficient of the integrand. The upper bound $x = 1 - y - z - t$ leads to the collinear divergence from l parallel to P_2, as stated before. It is easy to see that M^2 does not change sign in this term,

$$\begin{aligned} M^2_{x=1-y-z-t} &= (1-y-z-t)(y+z)k_1 \cdot (P_2 - k_2) \\ &\quad + y(1-y-z)k_1 \cdot k_2 - (1-y-z-t) \\ &\quad \times (y+z)k_1 \cdot k \\ &= (1-y-z-t)(y+z)k_1 \cdot (P_2 - k_2 - k) \\ &\quad + y(1-y-z)k_1 \cdot k_2 > 0, \end{aligned} \quad \text{(A2)}$$

due to the power counting $P_2^- - k_2^- \gg k^-$. Hence, it does not contribute to a Glauber divergence, and will be neglected. We then consider another term from the lower bound $x = 0$. Integrating out t, we obtain the second coefficient $1/(y+z)$ for the integrand. Similarly, the upper bound $t = 1 - y - z$ does not generate a Glauber divergence, because $M^2_{x=0;t=1-y-z} = y(1-y-z)k_1 \cdot k_2$ is always positive. We focus on the term from the lower bound $t = 0$,

$$M^2_{x,t=0} = (1-y-z)[yk_1 \cdot k_2 - (y+z)k_1 \cdot k]. \quad \text{(A3)}$$

For the power counting $k_2^- \sim O(m_B)$ and $k^- \sim O(\Lambda_{\rm QCD})$, it is obvious that the above expression can change sign in the infrared region $y \sim O(\lambda^2) \ll z \sim O(\lambda)$, where $\lambda \equiv \Lambda_{\rm QCD}/m_B$ denotes a small number. The above order of magnitude makes sense given the associated denominators $(k_2 - k + k_1 - l)^2 \sim O(m_B^2)$ and $(k - k_1 + l)^2 \sim O(m_B \Lambda_{\rm QCD})$. Therefore, Fig. 2(d) contributes to a Glauber divergence, as concluded in Sec. II.

Next we investigate Fig. 3(d) by associating the Feynman parameters x, t, z, and $1 - x - z - t$ with each of the denominators in Eq. (11) in sequence. Compared to Eq. (4), the parameter y is absent, and $P_2 - k_2$ in the first denominator is replaced by k_2. The corresponding M^2 is then written as

$$M^2 = xzk_1 \cdot k_2 - z(1-z-t)k_1 \cdot k. \quad \text{(A4)}$$

Integrating out x, we find the terms from the upper and lower bounds, $x = 1 - z - t$ and $x = 0$, respectively, cannot change sign:

$$\begin{aligned} M^2_{x=1-z-t} &= z(1-z-t)k_1 \cdot (k_2 - k) > 0, \\ M^2_{x=0} &= -z(1-z-t)k_1 \cdot k < 0, \end{aligned} \quad \text{(A5)}$$

for $k_2^- \gg k^-$ in our power counting. That is, Fig. 3(d) does not develop a Glauber divergence, as stated in Sec. II. Figures 2(d) and 3(d) have the same amplitudes in the soft region with $l \sim O(\Lambda_{\rm QCD})$ except for a sign difference, which is attributed to the emissions of the collinear gluon by the valence quark and valence antiquark in M_2. In the present analysis based on the Feynman parametrization, Fig. 3(d) provides soft subtraction for Fig. 2(d) at $y \to 0$. A convenient way to get the sum of Figs. 2(d) and 3(d) is to introduce a lower bound $y = y_{\rm min}$ for Eq. (A3). Obviously, Eq. (A3) still develops a Glauber divergence, as long as the hierarchy $y \ll z$ holds.

We turn to Fig. 2(f), which contains the five denominators

$$\begin{aligned} &[(P_2 - k_2 + l)^2 + i\epsilon][(k_1 - l)^2 + i\epsilon] \\ &\quad \times [(k - k_1 + l)^2 + i\epsilon](l^2 + i\epsilon) \\ &\quad \times [(k_2 - k + k_1 - l)^2 + i\epsilon]. \end{aligned} \quad \text{(A6)}$$

Associating the Feynman parameters x, t, z, $1 - x - y - z - t$, and y with each of the denominators in sequence, we have

$$M^2 = x(y+z+t)k_1 \cdot (P_2 - k_2) + y(1-y-z-t)k_1 \cdot k_2 - (1-y-z-t)(y+z)k_1 \cdot k, \quad \text{(A7)}$$

which is basically similar to Eq. (A1). We first integrate out x and get a power of $1/(y+z+t)$ as a coefficient of the integrand. The upper bound $x = 1 - y - z - t$ leads to a collinear divergence from l parallel to the P_2 meson. It is trivial to find that M^2 does not change sign in this term,

$$M^2_{x=1-y-z-t} = (1-y-z-t)[(y+z+t)k_1\cdot(P_2-k_2) + yk_1\cdot k_2-(y+z)k_1\cdot k], = (1-y-z-t)[(y+z)k_1\cdot(P_2-k_2-k) + tk_1\cdot(P_2-k_2)+yk_1\cdot k_2]>0, \quad \text{(A8)}$$

due to $P_2^- - k_2^- \gg k^-$. Hence, it does not contribute to a Glauber divergence, and will be neglected. Another term from the lower bound $x=0$ reads

$$M^2_{x=0} = (1-y-z-t)[yk_1\cdot k_2-(y+z)k_1\cdot k], \quad \text{(A9)}$$

which can change sign in the infrared region $y\sim O(\lambda^2)\ll z\sim O(\lambda)$, the same as for Eq. (A3); that is, Fig. 2(f) contributes to a Glauber divergence.

Correspondingly, we should investigate Fig. 3(f), which contains the four denominators

$$[(k_2+l)^2+i\epsilon][(k_1-l)^2+i\epsilon][(k-k_1+l)^2+i\epsilon](l^2+i\epsilon). \quad \text{(A10)}$$

The Feynman parameters x, t, z, and $1-x-z-t$ are associated with each of the denominators in sequence. Compared to Eq. (A6), the parameter y is absent, and P_2-k_2 in the first denominator is replaced by k_2. M^2 in this case is then written as

$$M^2 = x(z+t)k_1\cdot k_2 - z(1-z-t)k_1\cdot k. \quad \text{(A11)}$$

Integrating out x, we observe the terms from the upper and lower bounds, $x=1-z-t$ and $x=0$, respectively, cannot change sign,

$$M^2_{x=1-z-t} = (1-z-t)[tk_1\cdot k_2 + zk_1\cdot(k_2-k)]>0, \quad M^2_{x=0} = -z(1-z-t)k_1\cdot k<0 \quad \text{(A12)}$$

for $k_2^- \gg k^-$, and that Fig. 3(f) does not develop a Glauber divergence. Figure 3(f) just provides soft subtraction for Fig. 2(f) at $y\to 0$.

We then check the triple-gluon diagram in Fig. 2(e), which contains four denominators:

$$[(P_2-k_2+l)^2+i\epsilon][(k-k_1+l)^2+i\epsilon](l^2+i\epsilon) \times[(k_2-k+k_1-l)^2+i\epsilon]. \quad \text{(A13)}$$

Associating the Feynman parameters x, z, $1-x-y-z$, and y with each of the denominators in sequence, we have

$$M^2 = x(y+z)k_1\cdot(P_2-k_2)+y(1-y-z)k_1\cdot k_2 - (y+z)(1-y-z)k_1\cdot k. \quad \text{(A14)}$$

By integrating out x, the upper bound also gives a collinear divergence relevant to the M_2 meson, which does not change sign, just like Eq. (A2). The term from the lower bound $x=0$ reads

$$M^2_{x=0} = (1-y-z)[yk_1\cdot k_2-(y+z)k_1\cdot k], \quad \text{(A15)}$$

which is the same as for Figs. 2(d) and 2(f).

The Glauber divergence in Eq. (A15) can be isolated via the Ward identity in Eq. (10). Comparing the first term in Eq. (10) with Eq. (A13), the denominator $(k-k_1+l)^2+i\epsilon$ is replaced by $l^2+2(k-k_1)\cdot l+i\epsilon$. Therefore, the corresponding M^2 is given by

$$M^2 = x(y+z)k_1\cdot(P_2-k_2)+y(1-y-z)k_1\cdot k_2 - y(1-y-z)k_1\cdot k + z(y+z)k_1\cdot k, \quad \text{(A16)}$$

which can be derived simply by dropping the $-zk_1\cdot k$ term in Eq. (A14). The term from the lower bound $x=0$ corresponding to Eq. (A16) is then written as

$$M^2_{x=0} = y(1-y-z)k_1\cdot(k_2-k)+z(y+z)k_1\cdot k>0. \quad \text{(A17)}$$

Hence, the first term in Eq. (10), being free of a Glauber divergence, is absorbed into the M_2 meson wave function. It is found that the Glauber divergence in Fig. 2(e) has been moved into the second term in Eq. (10), which can be combined with those in Figs. 2(d) and 2(f). It turns out that the Glauber divergence associated with the M_2 meson has the color factor C_F, as was claimed in Ref. [29].

Consider all possible attachments of the collinear gluon emitted by the valence quark of M_1 to other particle lines, which are displayed in Fig. 14. Figure 14(c) contains the four denominators

$$[(k_2-l)^2+i\epsilon][(P_1-k_1+l)^2+i\epsilon](l^2+i\epsilon) \times[(k_2-k+k_1-l)^2+i\epsilon], \quad \text{(A18)}$$

with which the Feynman parameters x, t, $1-x-y-t$, and y are associated in sequence. It is straightforward to derive

$$M^2 = (x+y)t(P_1-k_1)\cdot k_2 + y(1-x-y)k_1\cdot k_2 - yt(P_1-k_1)\cdot k - y(1-y)k_1\cdot k. \quad \text{(A19)}$$

It is appropriate to integrate out t first, since its coefficient $x(P_1-k_1)\cdot k_2+y(P_1-k_1)\cdot(k_2-k)>0$ does not change sign according to the power-counting rules. The term from the upper bound $t=1-x-y$, which corresponds to a collinear divergence from l parallel to P_1, gives

$$M^2_{t=1-x-y} = (1-x-y)[(x+y)(P_1-k_1)\cdot k_2 + yk_1\cdot k_2 - y(P_1-k_1)\cdot k - yk_1\cdot k] - xyk_1\cdot k. \quad \text{(A20)}$$

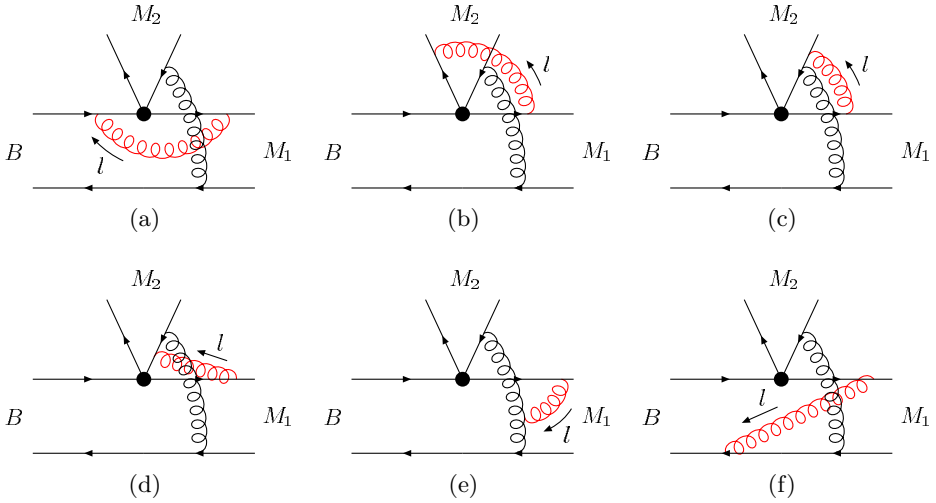

FIG. 14 (color online). NLO diagrams for Fig. 1(a) that are relevant to the factorization of the M_1 meson wave function.

To get pinched infrared singularities, we must have small x, y due to the large denominators $(k_2 - l)^2$, $(k_2 - k + k_1 - l)^2$. In the $x, y \to 0$ limit the above expression becomes

$$M^2_{t=1-x-y} = x(P_1 - k_1)\cdot k_2 + yP_1\cdot(k_2 - k) - xyk_1\cdot k > 0, \tag{A21}$$

because the third term over the first term is of $O(\lambda^3)$ even for $k_1^+ \sim O(m_B)$ [y is then of $O(\lambda^2)$]. Another term from the lower bound $t = 0$ is written as

$$\begin{aligned} M^2_{t=0} &= y[(1-x-y)k_1\cdot k_2 - (1-y)k_1\cdot k] \\ &\approx yk_1\cdot(k_2 - k) > 0 \end{aligned} \tag{A22}$$

in the $x, y \to 0$ limit. The pole structures of Eq. (A18) can be analyzed in the same way as in Sec. II. It will be seen that the interval of l^- does not cover the origin, as the contour integration over l^+ is performed first, or the Glauber divergences associated with the poles of l^- cancel each other at leading power in $1/m_B$ as l^- is integrated out first. In conclusion, Fig. 14(c) does not contain a Glauber divergence.

The analysis of Fig. 14(b) is trivial. Due to the absence of y, it is easy to write down

$$M^2 = xt(P_1 - k_1)\cdot(P_2 - k_2) > 0. \tag{A23}$$

That is, it just provides soft subtraction for Fig. 14(c) at $y \to 0$.

[1] Y. Amhis *et al.* (Heavy Flavor Averaging Group Collaboration), arXiv:1207.1158, and online update at http://www.slac.stanford.edu/xorg/hfag.
[2] C.-W. Chiang, M. Gronau, J. L. Rosner, and D. A. Suprun, Phys. Rev. D **70**, 034020 (2004); Y. Y. Charng and H.-n. Li, Phys. Rev. D **71**, 014036 (2005); R. Fleischer, S. Recksiegel, and F. Schwab, Eur. Phys. J. C **51**, 55 (2007).
[3] T. N. Pham, arXiv:0910.2561.
[4] H. Y. Cheng and C. K. Chua, Phys. Rev. D **80**, 074031 (2009).
[5] C. D. Lü and M. Z. Yang, Eur. Phys. J. C **23**, 275 (2002).
[6] R. Zhou, X. D. Gao, and C. D. Lü, Eur. Phys. J. C **72**, 1923 (2012).
[7] M. Beneke and M. Neubert, Nucl. Phys. **B675**, 333 (2003).
[8] H.-n. Li and S. Mishima, Phys. Rev. D **73**, 114014 (2006).
[9] W. S. Hou, H.-n. Li, S. Mishima, and M. Nagashima, Phys. Rev. Lett. **98**, 131801 (2007).
[10] A. Soni, A. K. Alok, A. Giri, R. Mohanta, and S. Nandi, Phys. Lett. B **683**, 302 (2010).
[11] R. Fleischer, S. Jager, D. Pirjol, and J. Zupan, Phys. Rev. D **78**, 111501 (2008) and references therein.
[12] S. Baek, J. H. Jeon, and C. S. Kim, Phys. Lett. B **664**, 84 (2008).
[13] G. Bhattacharyya, K. B. Chatterjee, and S. Nandi, Phys. Rev. D **78**, 095005 (2008).
[14] R. Mohanta and A. K. Giri, Phys. Rev. D **79**, 057902 (2009).
[15] Q. Chang, X.-Q. Li, and Y.-D. Yang, J. High Energy Phys. 05 (2009) 056.
[16] S. Baek, C.-W. Chiang, M. Gronau, D. London, and J. L. Rosner, Phys. Lett. B **678**, 97 (2009).
[17] S. Khalil, A. Masiero, and H. Murayama, Phys. Lett. B **682**, 74 (2009).
[18] K. Huitu and S. Khalil, Phys. Rev. D **81**, 095008 (2010).
[19] K. Cho and S.-h. Nam, Phys. Rev. D **88**, 035012 (2013).

[20] M. Imbeault, S. Baek, and D. London, Phys. Lett. B **663**, 410 (2008).
[21] M. Endo and T. Yoshinaga, Prog. Theor. Phys. **128**, 1251 (2012).
[22] M. Beneke, J. Rohrer, and D. Yang, Nucl. Phys. **B774**, 64 (2007).
[23] H. J. Lipkin, arXiv:1102.4700.
[24] Y. Y. Keum, H.-n. Li, and A. I. Sanda, Phys. Lett. B **504**, 6 (2001); Phys. Rev. D **63**, 054008 (2001).
[25] C. D. Lü, K. Ukai, and M. Z. Yang, Phys. Rev. D **63**, 074009 (2001).
[26] H.-n. Li, S. Mishima, and A. I. Sanda, Phys. Rev. D **72**, 114005 (2005).
[27] Y. L. Zhang, X. Y. Liu, Y. Y. Fan, S. Cheng, and Z. J. Xiao, Phys. Rev. D **90**, 014029 (2014).
[28] M. Beneke and D. Yang, Nucl. Phys. **B736**, 34 (2006); M. Beneke and S. Jager, Nucl. Phys. **B751**, 160 (2006); G. Bell, Nucl. Phys. **B795**, 1 (2008); V. Pilipp, Nucl. Phys. **B794**, 154 (2008); M. Beneke, T. Huber, and X. Q. Li, Nucl. Phys. **B832**, 109 (2010).
[29] H.-n. Li and S. Mishima, Phys. Rev. D **83**, 034023 (2011).
[30] J. Collins and J. W. Qiu, Phys. Rev. D **75**, 114014 (2007); J. Collins, arXiv:0708.4410.
[31] G. P. Lepage and S. J. Brodsky, Phys. Lett. **87B**, 359 (1979); S. Nussinov and R. Shrock, Phys. Rev. D **79**, 016005 (2009); M. Duraisamy and A. L. Kagan, Eur. Phys. J. C **70**, 921 (2010).
[32] M. Petric (Belle Collaboration), in *Proceedings of the 37th International Conference on High Energy Physics, Valencia, Spain, 2014* (to be published).
[33] C. K. Chua, W. S. Hou, and K. C. Yang, Phys. Rev. D **65**, 096007 (2002); A. B. Kaidalov and M. I. Vysotsky, Phys. Lett. B **652**, 203 (2007); M. I. Vysotsky, arXiv:0901.2245; A. F. Falk, A. L. Kagan, Y. Nir, and A. A. Petrov, Phys. Rev. D **57**, 4290 (1998).
[34] C. K. Chua, Phys. Rev. D **78**, 076002 (2008).
[35] C.-p. Chang and H.-n. Li, Eur. Phys. J. C **71**, 1687 (2011); H.-n. Li, arXiv:1009.3610.
[36] M. Nagashima and H.-n. Li, Phys. Rev. D **67**, 034001 (2003).
[37] H.-n. Li, Y. L. Shen, and Y. M. Wang, Phys. Rev. D **85**, 074004 (2012).
[38] G. Buchalla, A. J. Buras, and M. E. Lautenbacher, Rev. Mod. Phys. **68**, 1125 (1996).
[39] H.-n. Li and B. Tseng, Phys. Rev. D **57**, 443 (1998).
[40] H.-n. Li, Phys. Rev. D **64**, 014019 (2001).
[41] H.-n. Li and S. Mishima, Phys. Rev. D **74**, 094020 (2006).
[42] Below Eq. (6) in Ref. [41], the distribution amplitude $(-\phi_s^M)$ has to be corrected to $(+\phi_M^s)$.
[43] J. Beringer *et al.* (Particle Data Group), Phys. Rev. D **86**, 010001 (2012), and online update at http://pdg.lbl.gov/.
[44] P. Ball, G. W. Jones, and R. Zwicky, Phys. Rev. D **75**, 054004 (2007).
[45] T. Kurimoto, H.-n. Li, and A. I. Sanda, Phys. Rev. D **65**, 014007 (2001).
[46] M. Ciuchini, E. Franco, G. Martinelli, M. Pierini, and L. Silvestrini, Phys. Lett. B **674**, 197 (2009).
[47] S. Baek, C.-W. Chiang, and D. London, Phys. Lett. B **675**, 59 (2009).
[48] C.-p. Chang and H.-n. Li, Phys. Lett. B **726**, 262 (2013).
[49] C. S. Lam and W. K. Tung, Phys. Rev. D **18**, 2447 (1978).
[50] S. Falciano *et al.* (NA10 Collaboration), Z. Phys. C **31**, 513 (1986).
[51] M. Guanziroli *et al.* (NA10 Collaboration), Z. Phys. C **37**, 545 (1988).
[52] J. S. Conway *et al.*, Phys. Rev. D **39**, 92 (1989).
[53] L. D. Landau, Nucl. Phys. **13**, 181 (1959).